NMRF/VR/02/2024

VERIFICATION REPORT

NCUM Global Model Verification: Winter (DJF) 2023-24

K. Niranjan Kumar, Sukhwinder Kaur, Mohana S. Thota, M. Venkatarami Reddy, Harvir Singh, Sushant Kumar, Anumeha Dube, Sumit Kumar, and Raghavendra Ashrit

2024

National Centre for Medium-Range Weather Forecasting
Ministry of Earth Sciences, Government of India
A-50, Sector-62, NOIDA-201 309, INDIA

NCUM Global Model Verification:
Winter (DJF) 2023-24

K. Niranjan Kumar, Sukhwinder Kaur, Mohana S. Thota, M. Venkatarami Reddy, Harvir Singh, Sushant Kumar, Anumeha Dube, Sumit Kumar, and Raghavendra Ashrit

NMRF/VR/02/2024

National Centre for Medium-Range Weather Forecasting
Ministry of Earth Sciences, Government of India
A-50, Sector 62, NOIDA-201309, INDIA
www.ncmrwf.gov.in

Data Control Sheet

1	Name of the Institute	National Center for Medium-Range Weather Forecasting
2	Document Number	NMRF/VR/02/2024
3	Date of Publication	July 2024
4	Title of the document	NCUM Global Model Verification: Winter (DJF) 2023-24
5	Type of the document	Verification Report
6	Number of pages, figures, and Tables	46 pages, 34 figures, 4 Tables (including Appendix Figures and Tables)
7	Author (S)	K. Niranjan Kumar, Sukhwinder Kaur, Mohana S. Thota, M. Venkatarami Reddy, Harvir Singh, Sushant Kumar, Anumeha Dube, Sumit Kumar, and Raghavendra Ashrit
8	Originating Unit	National Centre for Medium-Range Weather Forecasting (NCMRWF), A-50, Sector-62, NOIDA201 309, India
9	Abstract	This report documents the performance of the global NCMRWF Unified Model (NCUM-G) analysis and forecast during the winter season (DJF) 2022-23. The verification results are presented to address both forecasters and model developers. The information on biases in the forecasted winds, temperature, humidity, rainfall, etc., is crucial for the forecasters to interpret the model guidance for accurate forecasting. Additionally, information on recent improvements in the model's skill contributes to strengthening confidence in the accuracy of the model forecasts.
10	References	17
11	Security classification	Unrestricted
12	Distribution	General

Table of Contents

NMRF/VR/02/2024

NCUM Global Model Verification:

Winter (DJF) 2023-24

K. Niranjan Kumar, Sukhwinder Kaur, Mohana S. Thota, M. Venkatarami Reddy, Harvir Singh, Sushant Kumar, Anumeha Dube, Sumit Kumar, and Raghavendra Ashrit

सारांश

यह रिपोर्ट सर्दियों के मौसम (दिसंबर से फरवरी) 2023-24के दौरान वैश्विक रा.म.अ.मौ.पू.कें. यूनिफाइड मॉडल (एन.सी.यू.एम.-जी) विश्लेषण और पूर्वानुमान के प्रदर्शन का दस्तावेजीकरण करती है। सत्यापन परिणाम पूर्वानुमानकर्ताओं और मॉडल डेवलपर्स दोनों को संबोधित करने के लिए प्रस्तुत किए जाते हैं। सटीक पूर्वानुमान के लिए मॉडल मार्गदर्शन की व्याख्या करने के लिए पूर्वानुमानकर्ताओं के लिए पूर्वानुमानित हवाओं, तापमान, आर्द्रता, वर्षा आदि में पूर्वाग्रहों की जानकारी महत्वपूर्ण है। इसके अतिरिक्त, मॉडल के कौशल में हाल के सुधारों की जानकारी मॉडल पूर्वानुमानों की सटीकता में विश्वास बढ़ाने में योगदान देती है।

Abstract

This report documents the performance of the global NCMRWF Unified Model (NCUM-G) analysis and forecast during the winter season (DJF) 2023-24. The verification results are presented to address both forecasters and model developers. The information on biases in the forecasted winds, temperature, humidity, rainfall, etc., is crucial for the forecasters to interpret the model guidance for accurate forecasting. Additionally, information on recent improvements in the model's skill contributes to strengthening confidence in the accuracy of the model forecasts.

1. Introduction

This report documents the performance of the global NCMRWF Unified Model (NCUM-G) forecasts during the winter season (DJF) of 2023-24. The key objective of this assessment is to verify the forecasts' accuracy and reliability by comparing them to model analyses and observations. The results are summarized for the winter season to understand the average biases and forecast performances. The report is oriented towards both forecasters and model developers. Section 2 of the report elucidates the NCUM-G model description and the data assimilation system at NCMRWF, along with detailing the observed data utilized in this study. A comprehensive study of the seasonal mean analysis and corresponding anomalies is given in section 3, providing readers with a holistic view of the model's performance during the winter season. Section 4 delves into the systematic biases observed in the forecasted large-scale upper fields, specifically focusing on wind, temperature, humidity, rainfall, etc., which are expected to be useful for the forecasters to interpret the model forecasts, followed by a detailed validation of forecasts in section 5. Section 6 touches upon verification for significant weather events of DJF 2023-24. This includes verification for the Bay of Bengal (BoB) Severe Cyclonic Storm (SCS) 'Michaung' during 01-06 Dec 2023, which made landfall at Bapatla (in Andhra Pradesh) on 5th Dec 2023. Section 7 provides a concise summary of the results.

2. NCMRWF Unified Modelling System & Verification datasets

2.1. Model Description

The NCMRWF started using the Unified Model (UM) Partnerships' seamless prediction system since 2012, designating it as NCUM. The operationalization of the NCMRWF global Numerical Weather Prediction (NWP) system (NCUM-G) commenced in 2012 with a grid resolution of 25 km (NCUM-G: V1) specifically tailored for medium-range weather prediction. This system underwent several upgrades, progressing to a 17 km horizontal resolution (NCUM-G: V3) in 2015, followed by further refinement to a 12 km resolution (NCUM-G: V5) in 2018. Subsequently, in 2020, the system transitioned to a 12 km resolution with enhanced model physics, designated as NCUM-G: V6. The present version (NCUM-G: V7) of NCUM-G has a horizontal grid resolution of ~12 km with 70 levels in the atmosphere reaching 80 km height. It uses an "ENDGame" dynamical core, which provides improved accuracy of the solution of primitive model equations and reduced damping. This helps in producing finer details in the simulations of synoptic features such as cyclones, fronts, troughs, and jet stream winds. ENDGame also increases variability in the tropics, which leads to an improved representation of tropical cyclones and other tropical phenomena. The model uses improved physics options of GA7.2 (Walters et al., 2017). An advanced data assimilation method of Hybrid 4-Dimensional Variational (4D-Var) is used for the creation of NCUM global analysis. The advantage of the

Hybrid 4D-Var is that it uses a blended background error, a blend of "climatological" background error, and day-to-day varying flow-dependent background error (derived from the 22–member ensemble forecasts). The hybrid approach is scientifically attractive because it elegantly combines the benefits of ensemble data assimilation (flow-dependent co-variances) with the known benefits of 4D-Var within a single data assimilation system (Barker, 2011). A brief description of the NCUM Hybrid 4D-Var system is given by Kumar et al. (2021, 2020, & 2019).

2.2. Observed/analysis Data used for the Verification

The study employs the fifth-generation European Centre for Medium-Range Weather Forecasts (ECMWF) reanalysis product, known as ERA-5, to analyze seasonal means and anomalies across the period from 1979 to 2018 (Hershbach et al. (2020)). This analysis utilizes high-resolution (12km) NCUM-G data, which is then interpolated to match the ERA-5 grid resolution of 0.250 x 0.250. To ensure the accuracy of forecasts, the NCUM-G model analysis serves as the basis for verification. Additionally, all systematic errors are calculated at the native 12km grid resolution.

For a comprehensive quantitative assessment of rainfall forecasts, the India Meteorological Department (IMD)-NCMRWF daily high-resolution (0.250) rainfall analysis is utilized, as outlined by Mitra et al. (2009, 2013). This analysis involves objectively integrating IMD's daily rain gauge observations onto a 0.250 grid through a successive corrections technique, with initial estimates derived from the GPM Satellite rainfall data. The model forecasts are then aligned with the observed rainfall grids over Indian land areas, covering a period from December 1, 2023, to February 29, 2024. According to Mitra et al. (2009), employing a merged analysis at a 0.250 grid resolution is crucial for accurately representing the large-scale rain characteristics typical of the monsoon season. Furthermore, blending IMD gauge measurements with GPM estimates helps rectify mean biases in satellite-derived data and enhances the representation of large-scale spatial patterns, mitigating the impact of temporal sampling errors (Mitra et al. 2009). Lastly, the verification of daily temperature forecasts is conducted using IMD's observed gridded data for maximum (Tmax) and minimum (Tmin) temperatures, with a grid resolution of 0.50 x 0.50, as per
Srivastava et al. (2009).

3. NCUM-G Analysis Mean and Anomalies during DJF 2023-24

3.1. Winds at 850, 700, 500, and 200 hPa levels

In this section, we evaluate the NCUM-G model's mean analysis fields and their anomalies in relation to climatology during the winter season of 2023-24, focusing on the dynamics of winds, temperature, and relative humidity across four standard pressure levels: 850, 700, 500, and 200 hPa. These analyses are benchmarked against the ERA5 climatology dataset spanning from 1979 to 2018. The findings, including mean winds and anomalies at 850 and 700 hPa, are illustrated in Figures 1a-d. At these levels, the predominant weather patterns encompass northeasterly winds across southern peninsular India and easterly winds over the southern Bay of Bengal. The westerly winds observed on the polar side of the low-level anticyclone in central India exhibit increased velocity with height, peaking at 8-10 m/s at 700 hPa (as seen in Figures 1a and 1b). This wind pattern likely facilitates moisture transport from the Arabian Sea (AS), enhancing precipitation potential in conjunction with Western Disturbances (WDs). Furthermore, the NCUM-G model analysis identifies a prominent low-level anticyclonic circulation characteristic of winter in central India.

To quantify the anomalous conditions specific to the winter of 2023-24, we subtract the climatological ERA5 reanalysis from the NCUM-G seasonal mean winds. The resulting mean anomalous winds at 850 and 700 hPa are displayed in Figures 1c-d. These anomalies reveal distinct patterns between the northern and southern regions of the Indian subcontinent, with the NCUM-G analysis showing either stronger or weaker winds compared to the ERA5 reanalysis, depending on the location. Interestingly, the equatorial Indian Ocean, particularly in its southern latitudes, experiences notably weaker winds according to the NCUM-G analysis. Moreover, in northwest India, where winter rainfall is typically higher, the wind magnitudes are found to be comparatively lower than those indicated by the ERA5 reanalysis, attributed to the persistence of anomalous easterlies (as depicted in Figure 1).

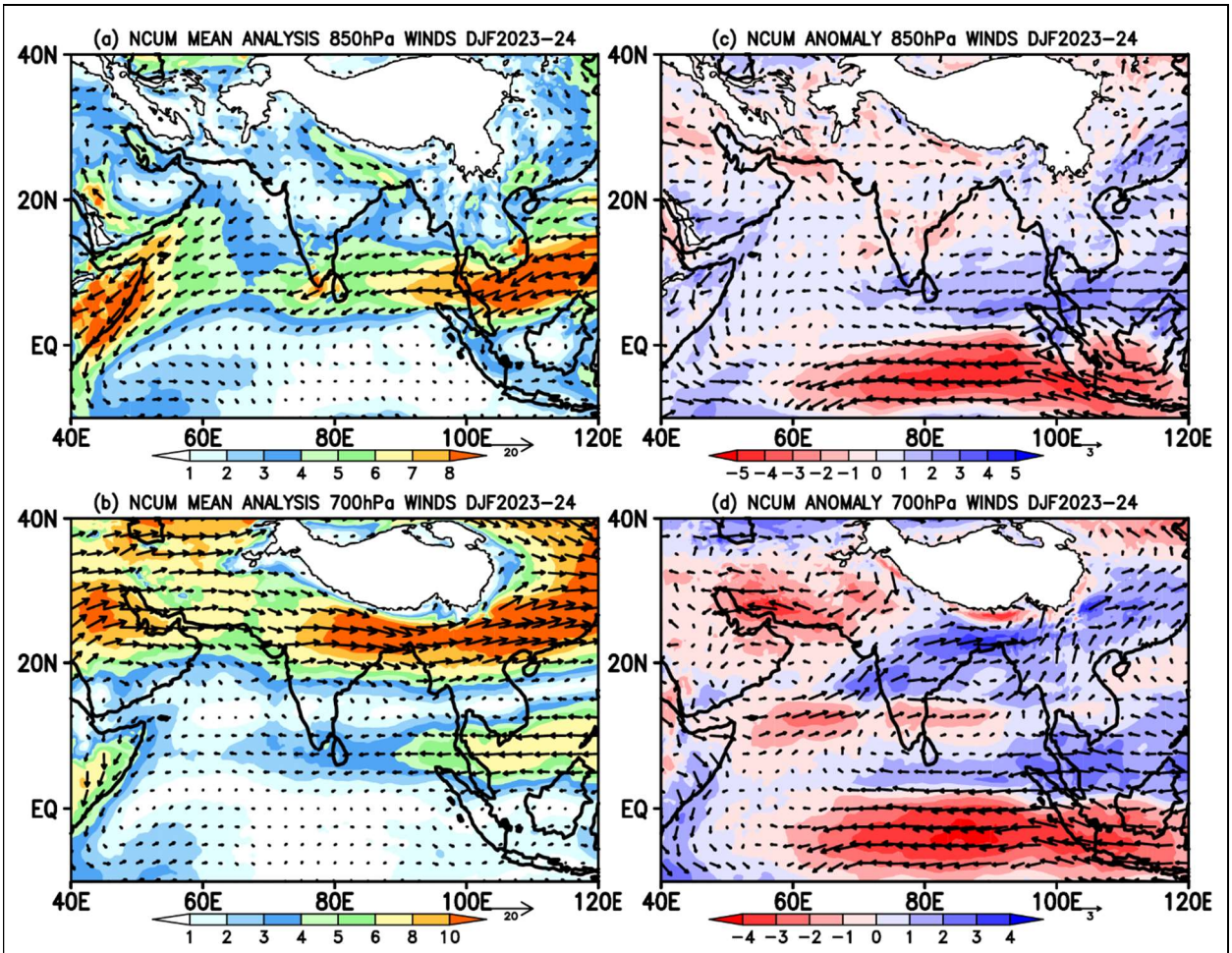

Figure 1. Mean winds at (a) 850 hPa and (b) 700 hPa in the NCUM-G Analysis during DJF 2023-24 (m/s). Right panels show the anomaly circulations at (c) 850 hPa and (d) 700 hPa.

The mean winds derived from the NCUM-G model analysis at both 500 hPa and 200 hPa levels, indicative of the mid-to-upper troposphere, are depicted in Figures 2a and 2b, respectively. As altitude increases, the mean winds within the northern Indian region experience significant strengthening, rising from approximately 16 m/s at 500 hPa to over 40 m/s in the upper troposphere. The NCUM-G model effectively captures the magnitude of the subtropical westerly jet (STWJ) winds across mid and upper atmospheric layers. This phenomenon represents a crucial seasonal quasi-permanent synoptic system, contributing substantially to precipitation through interactions with eastward-moving Western Disturbances (WDs). Conversely, the southern Indian region exhibits weaker easterly winds, as evident in Figures 2a and 2b. The model analysis also highlights the anomalous winds in Figures 2c and 2d. Notably, these anomalous winds are significantly stronger over the northern Indian region compared to the southern region in the mid-to-upper troposphere. Additionally, the presence of an anomalous mid-troposphere cyclone leads to prevailing westerly anomalies over the Bay of Bengal. In the equatorial zones, the upper tropospheric winds exhibit robust strength over the

western equatorial areas, contrasting with their relative weakness over the eastern equatorial regions during the winter of 2023-24.

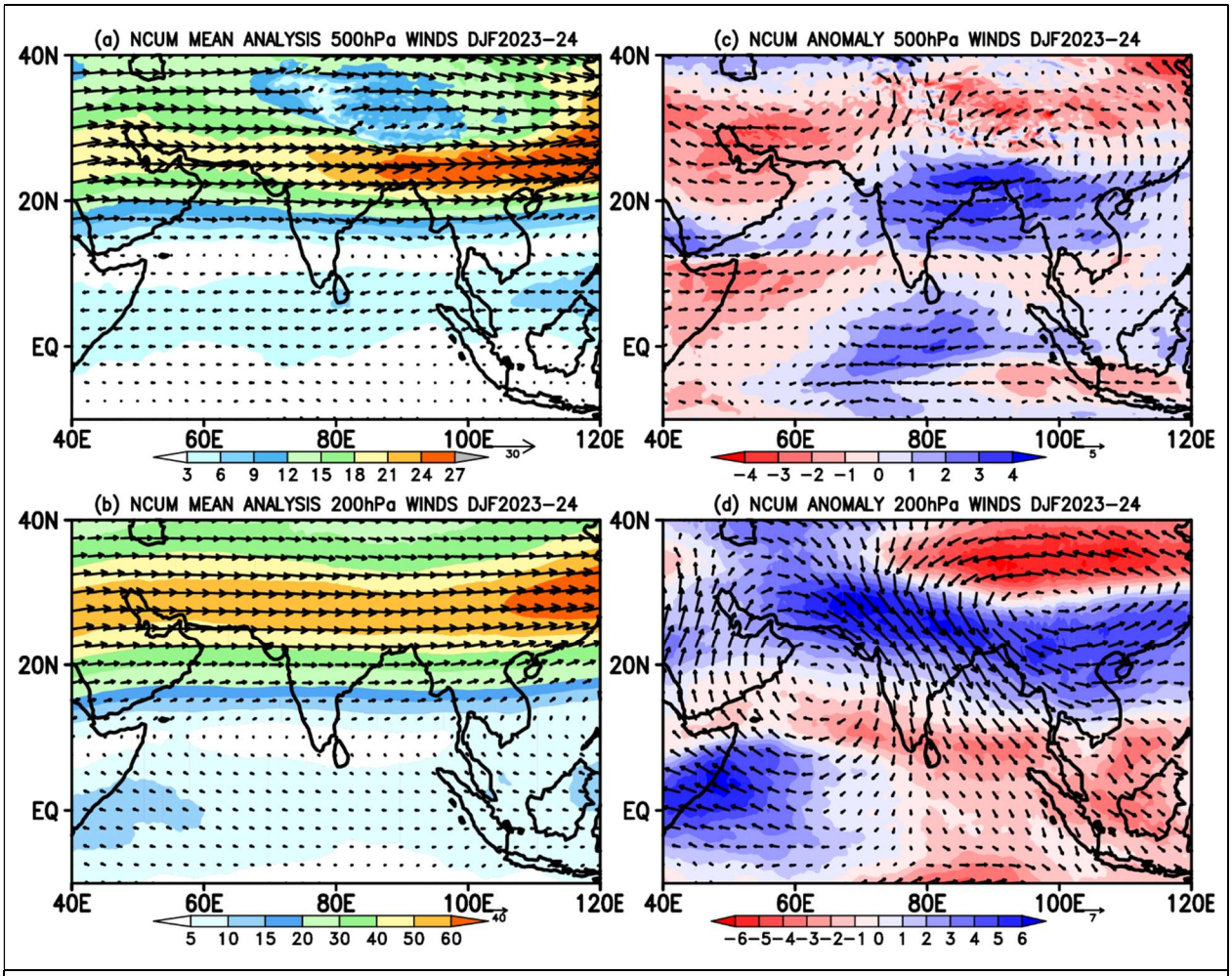

Figure 2. Mean winds at (a) 500 hPa and (b) 200 hPa in the NCUM-G Analysis during DJF 2023-24(m/s). Right panels show the anomaly circulations at (c) 500 hPa and (d) 200 hPa.

3.2. Temperature at 850, 700, 500, and 200 hPa levels

Figure 3 illustrates the spatial distribution of seasonal mean temperature. Typically, the colder season begins around mid-November in northern India, with December and January being the coldest months in the northern plains. Throughout these months, the average daily temperature typically falls below 20°C in most areas of northern India, as depicted in Figure 3a. Conversely, moving from north to south across the Peninsular region of India, temperatures generally increase, reflecting this pattern in Figure 3a. Similar spatial trends are observable in the daily mean temperatures at an altitude of 700 hPa, as shown in Figure 3b.

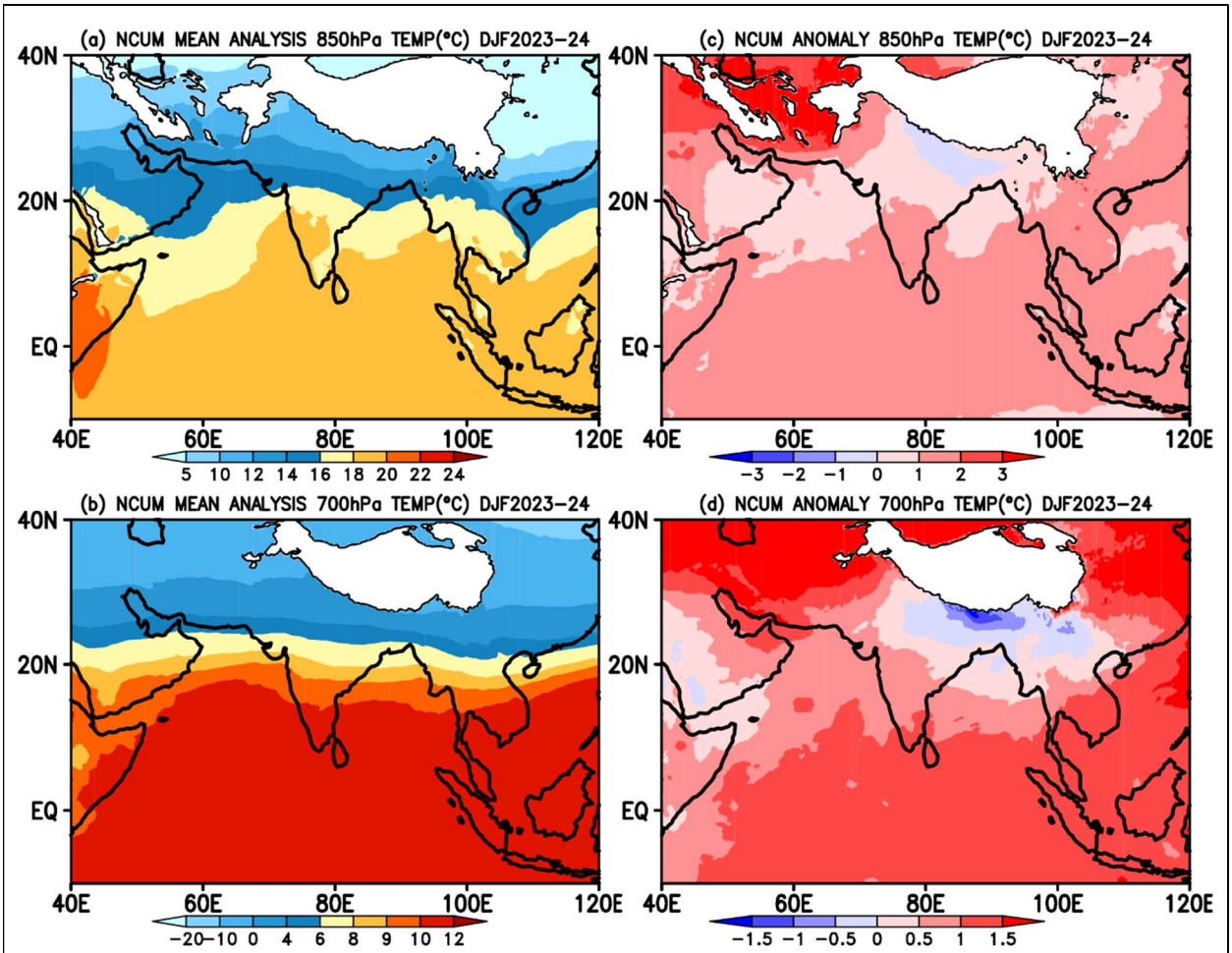

Figure 3. Mean Temperature (Degree Celsius, ºC) at (a) 850 hPa and (b) 700 hPa in the NCUM-G Analysis during DJF 2023-24. Right panels show the Temperature anomalies at (c) 850 hPa and (d) 700 hPa.

Anomalies in temperature within the lower troposphere, specifically at 850 hPa and 700 hPa (as indicated in Figures 3c and 3d), suggest that the winter of 2023-24 was warmer than usual, with temperature deviations ranging between 1-2°C in northern India. These warmer temperatures extend from northwest to southeast India, except for the Indo-Gangetic plains. The elevated temperatures in the northern and central regions of India are attributed to a large-scale adiabatic descent caused by anticyclonic circulation, which spans from 850 to 200 hPa levels. As one ascends in atmospheric pressure levels, the mean temperature distribution at both 500 hPa and 200 hPa significantly declines, as evident in Figures 4a and 4b. At 200 hPa, temperatures appear relatively uniform across the nation. However, despite this overall trend, temperature anomalies in northern India still indicate that the region experienced warmer-than-usual conditions during this period, as further illustrated in Figures 4c and 4d.

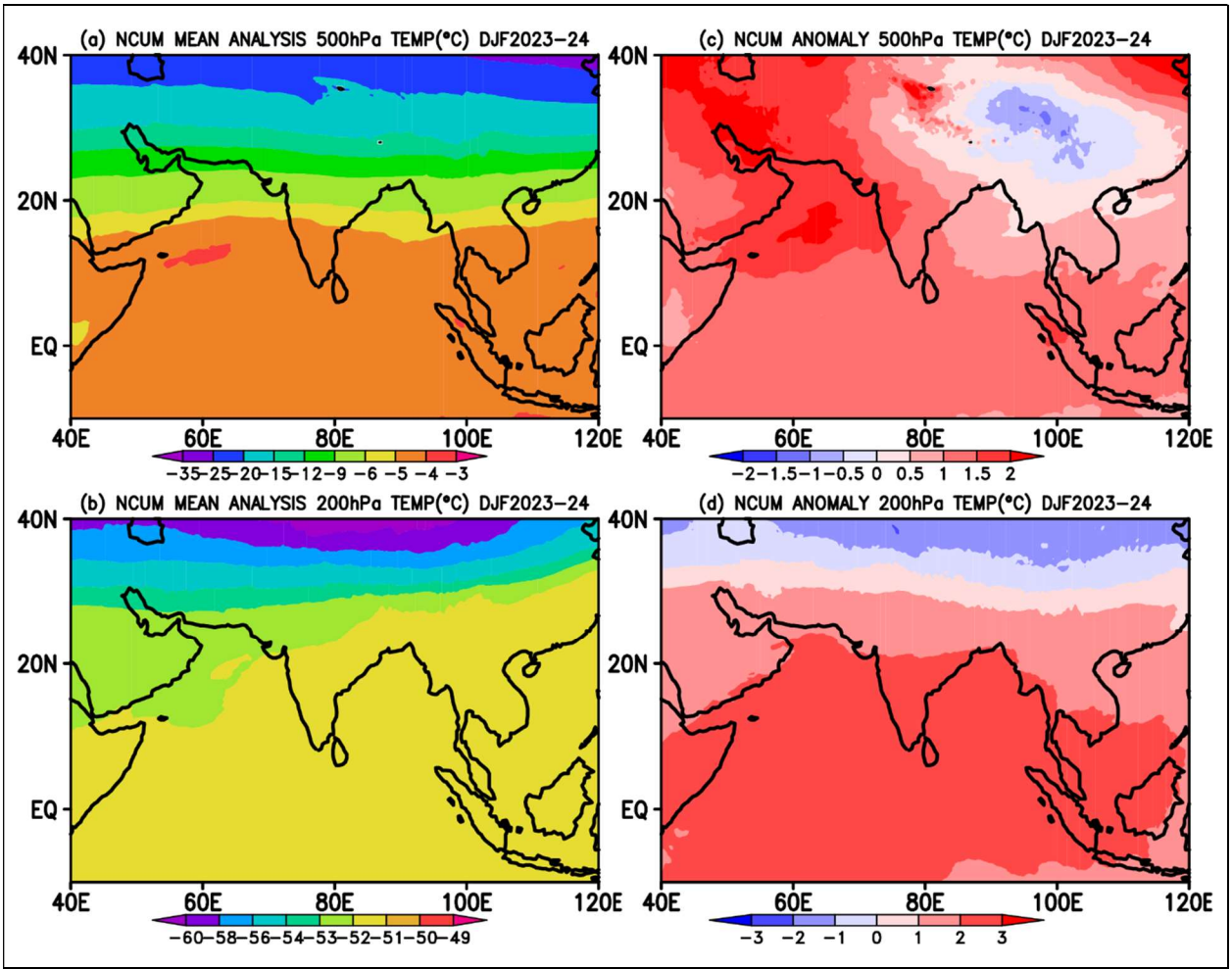

Figure 4. Mean Temperature (Degree Celsius, ºC) at (a) 500 hPa and (b) 200 hPa in the NCUM-G Analysis during DJF 2023-24. Right panels show the Temperature anomalies at (c) 500 hPa and (d) 200 hPa.

3.3. Relative Humidity (RH) at 850, 700, and 500 hPa levels

The interplay between humidity distribution, wind patterns, and temperature significantly impacts rainfall distribution. Figures 5a and 5b, derived from the NCUM-G model analysis, depict the seasonal mean relative humidity (RH) spatial patterns at 850 hPa and 700 hPa levels, respectively. During the winter season, India's northern regions encounter drier air masses originating from the cold north, leading to lower RH values at 850 hPa, as shown in Figure 5a. Conversely, the southern parts exhibit higher RH levels at the same altitude. At the 700 hPa level, most of the Indian subcontinent experiences dry conditions, as illustrated in Figure 5b.

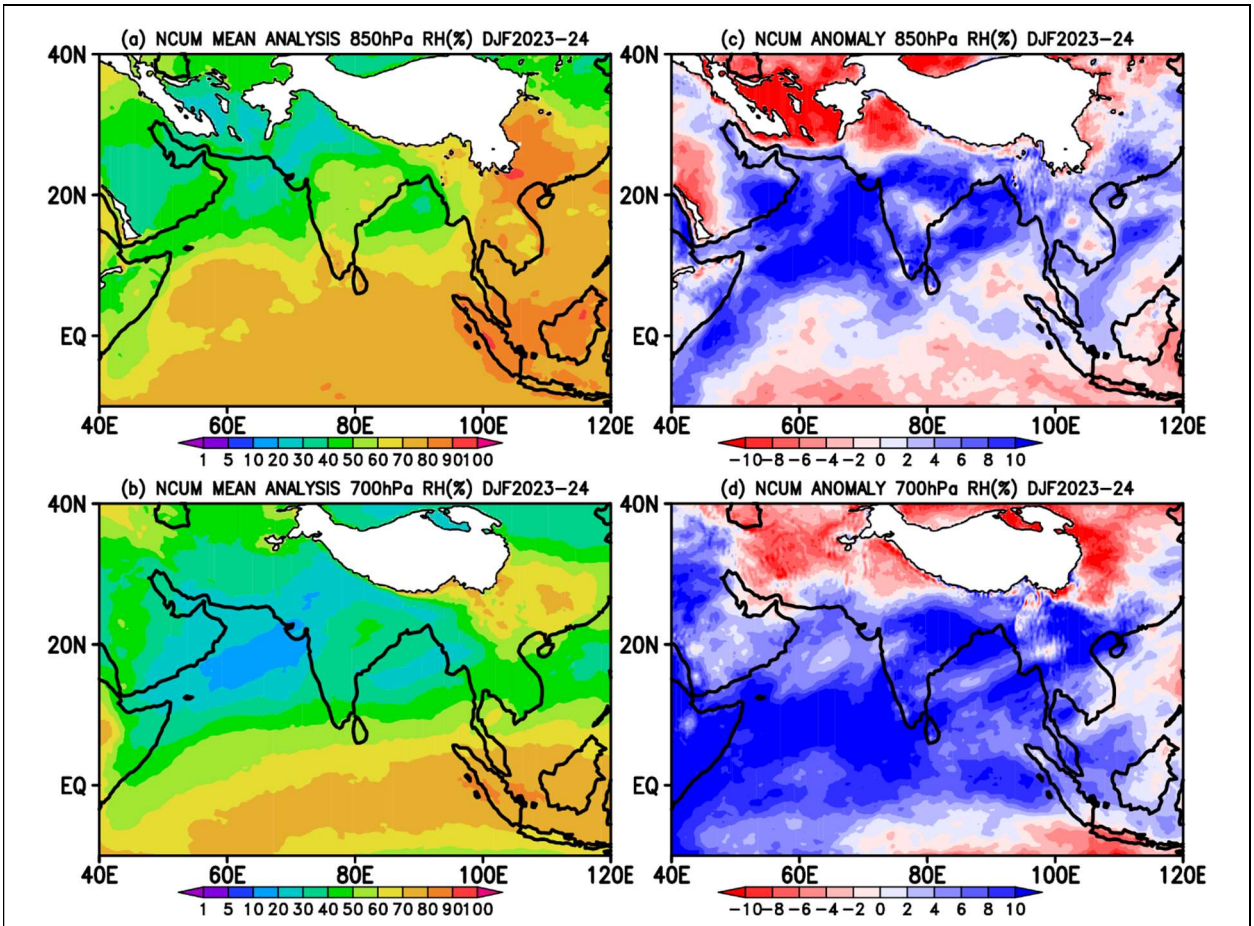

Figure 5. Mean Relative Humidity (%) at (a) 850 hPa and (b) 700 hPa in the NCUM-G Analysis during DJF 2023-24. The right panels show the anomalies in Relative Humidity at (c) 850 hPa and (d) 700 hPa.

An examination of anomalies indicates that the December-January-February (DJF) period of 2023-24 witnessed an overall increase in RH percentages across India, with the exception of certain northern territories, as evidenced in Figures 5c and 5d. Additionally, the Bay of Bengal and Arabian Seas exhibited positive humidity anomalies throughout the winter months. This contrasts with the equatorial regions, which experienced negative anomalies at 850 hPa and varied anomalies at 700 hPa levels.

Additionally, Figure 6 presents the spatial distribution of relative humidity (RH) in the mid-troposphere at the 500 hPa level. The seasonal mean RH distribution reveals dry conditions across the Indian Subcontinent. However, during the winter in northern India, the presence of synoptic-scale disturbances can temporarily elevate RH levels significantly. These increases in RH, indicative of excess moisture in the atmosphere, promote thermodynamic instability, thereby facilitating convective activity. Conversely, in oceanic regions, particularly the Maritime Continent, there is a notable presence of moisture, with RH exceeding 60%. Figure 6 (right panel) illustrates the anomalous RH distribution. While the southern Indian region exhibits slight

positive RH anomalies relative to climatology, these are not substantial given the region's already low mean RH. In contrast, the Maritime Continent displays negative RH anomalies, despite its generally higher mean RH distribution.

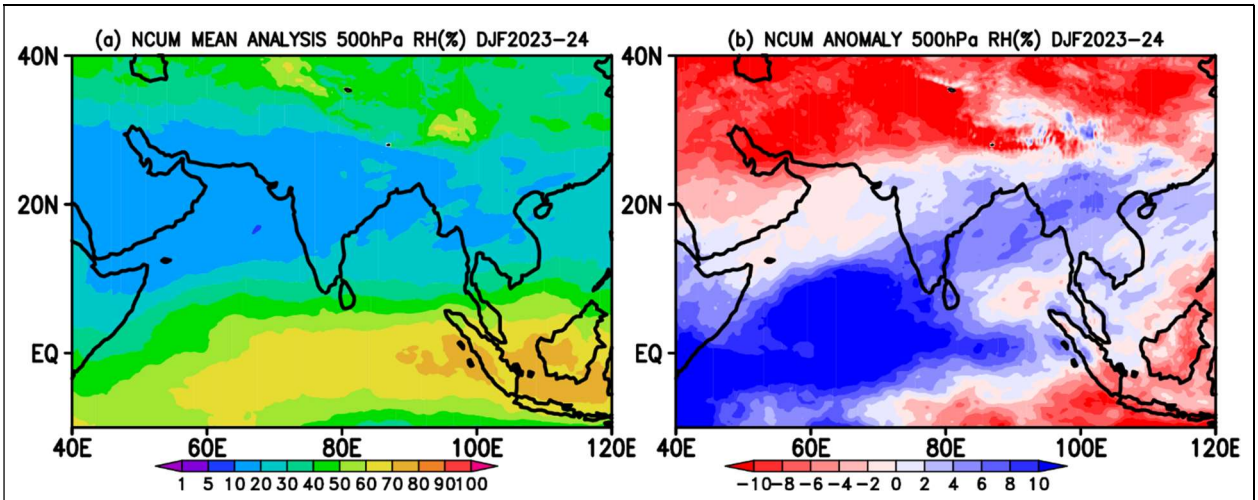

Figure 6: Mean Relative Humidity (%) at (a) 500 hPa in the NCUM-G Analysis during DJF 2023-24. The right panel shows the anomalies in Relative Humidity at (b) 500 hPa.

4. Systematic Errors in NCUM-G Forecasts

In this section, the systematic errors in Day-1 (24 hr), Day-3 (72 hr), and Day-5 (120 hr) forecasts during DJF 2023-24 are briefly described. In addition, the forecast errors with respect to model analysis are also presented for Winds and Temperature at 850, 700, 500, and 200 hPa levels; and Relative Humidity at 850 and 700 hPa levels (Figures 7-16).

4.1. Winds at 850, 700, 500, and 200 hPa levels

At the atmospheric level of 850 hPa, the mean wind patterns highlight the presence of anticyclonic circulation centered over central India, characterized by westerly winds in the north and easterly winds in the south. The Bay of Bengal and Arabian Sea regions are dominated by northeasterly winds, with the most intense winds observed along the coasts of Somalia and the South China Sea. Analysis of systematic errors in wind forecasts starting from Day-1 at this altitude shows westerly bias over the northern Arabian sea with magnitude increasing with lead time and an easterly bias over the southern Bay of Bengal. Similar trends in systematic wind-related errors are also noted at the 700 hPa level, with Day-1 forecast errors being less significant compared to those for Day-3 and Day-5 forecasts, as shown in Figures 8b-d. Furthermore, a more distinct westward wind bias emerges at the 700 hPa level over central India and the northeastern regions in forecasts

extending to Day-3 and Day-5, illustrated in Figures 8c-d. Further, over the equatorial regions a westerly bias is evident and the errors tend to amplify as the forecast lead time increases, possibly due to enhanced convective activity in equatorial areas during the winter season, as depicted in Figures 8b-d.

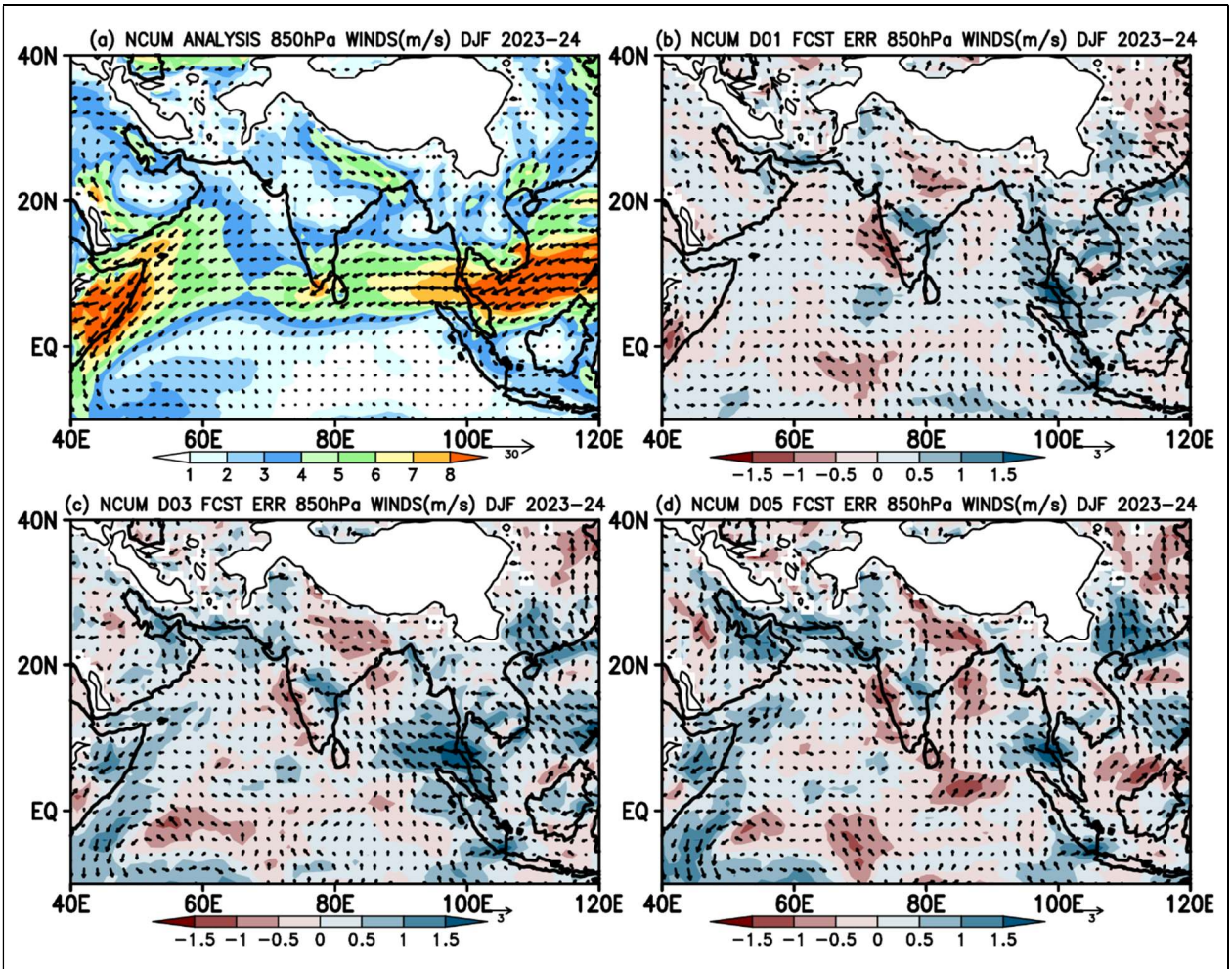

Figure 7. (a) Mean winds and systematic errors (m/s) in (b) Day-1, (c) Day-3, and (d) Day-5 forecasts at 850 hPa during DJF 2023-24.

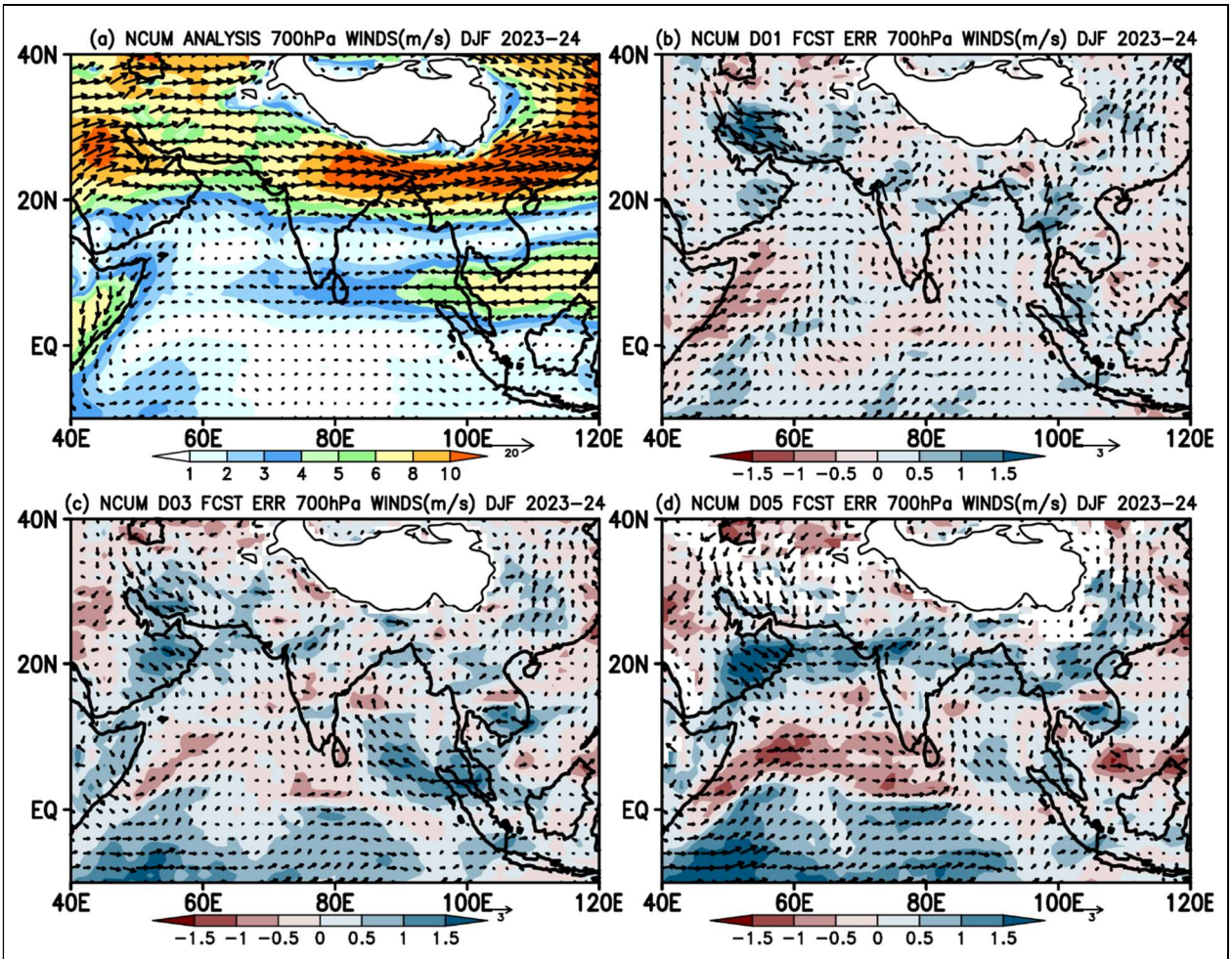

Figure 8. (a) Mean winds and systematic errors (m/s) in (b) Day-1, (c) Day-3, and (d) Day-5 forecasts at 700 hPa during DJF 2023-24

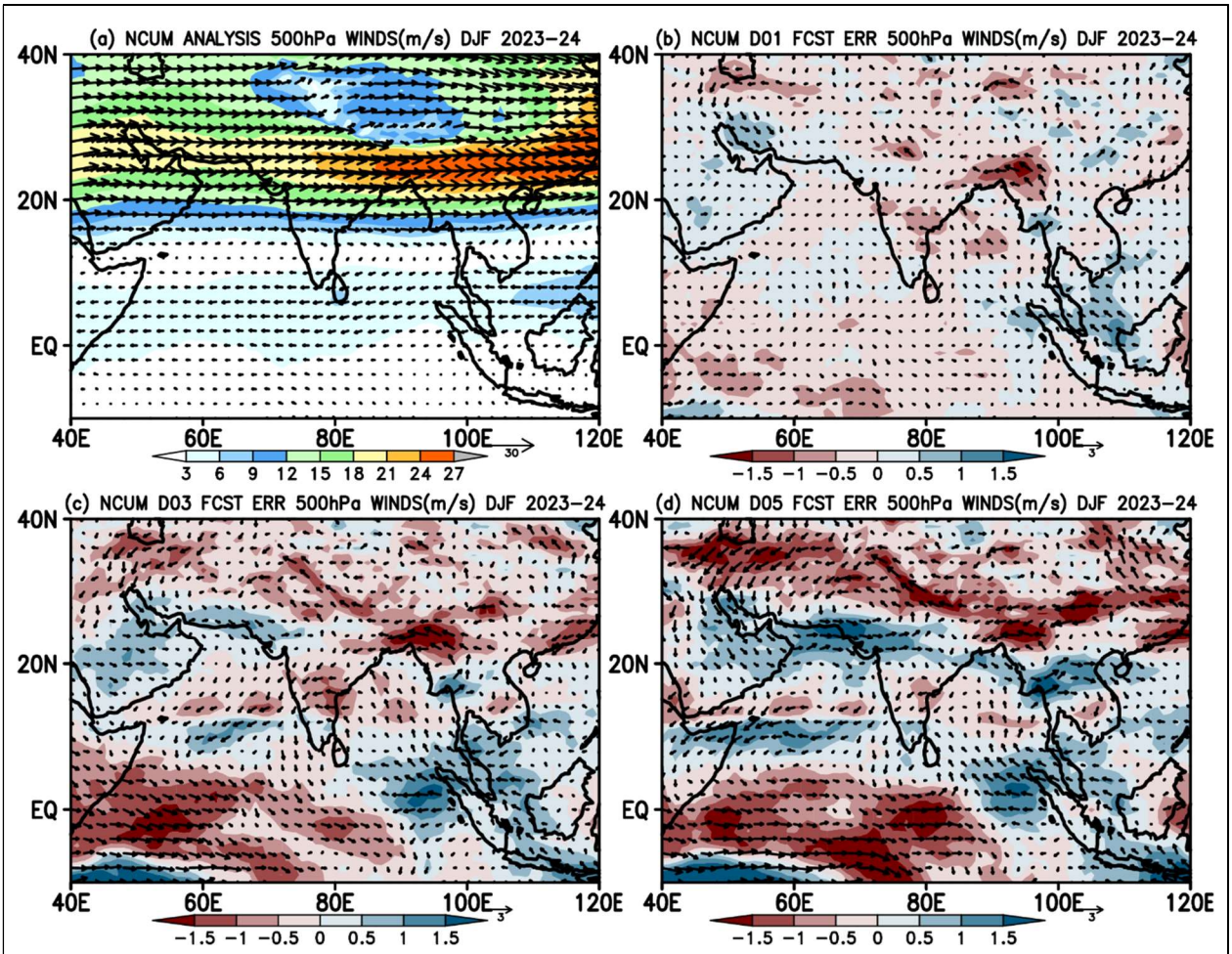

Figure 9. (a) Mean winds and systematic errors (m/s) in (b) Day-1, (c) Day-3, and (d) Day-5 forecasts at 500 hPa during DJF 2023-24.

At the 500 hPa atmospheric level, as illustrated in Figure 9a, robust westerly winds are observed between latitudes 30°N and 40°N, extending over the central Indian region. Initial forecasts on Day-1 for this level exhibit minimal errors in wind predictions. However, as the forecast period extends to Day-3 and Day-5, there is a noticeable enhancement in the westerly wind bias over the northern parts of India and an easterly wind bias over the southern Bay of Bengal and the Arabian Sea. By Day-5, these intensified winds contribute to the formation of cyclonic circulation just north of the equator around the 500 hPa level, a significant observation captured in Figures 9b-d.

Meanwhile, systematic errors in wind forecasts at the 200 hPa level reveal an increase in divergent circulation centered around the Head Bay and adjacent land areas by Day-3, with a similar spatial distribution persisting into Day-5 forecasts but with amplified error magnitudes, as depicted in Figures 10c-d. This enhancement in divergent circulations over the Bay and will impact the strengthening or weakening of the subtropical westerlies as the forecast lead time increases.

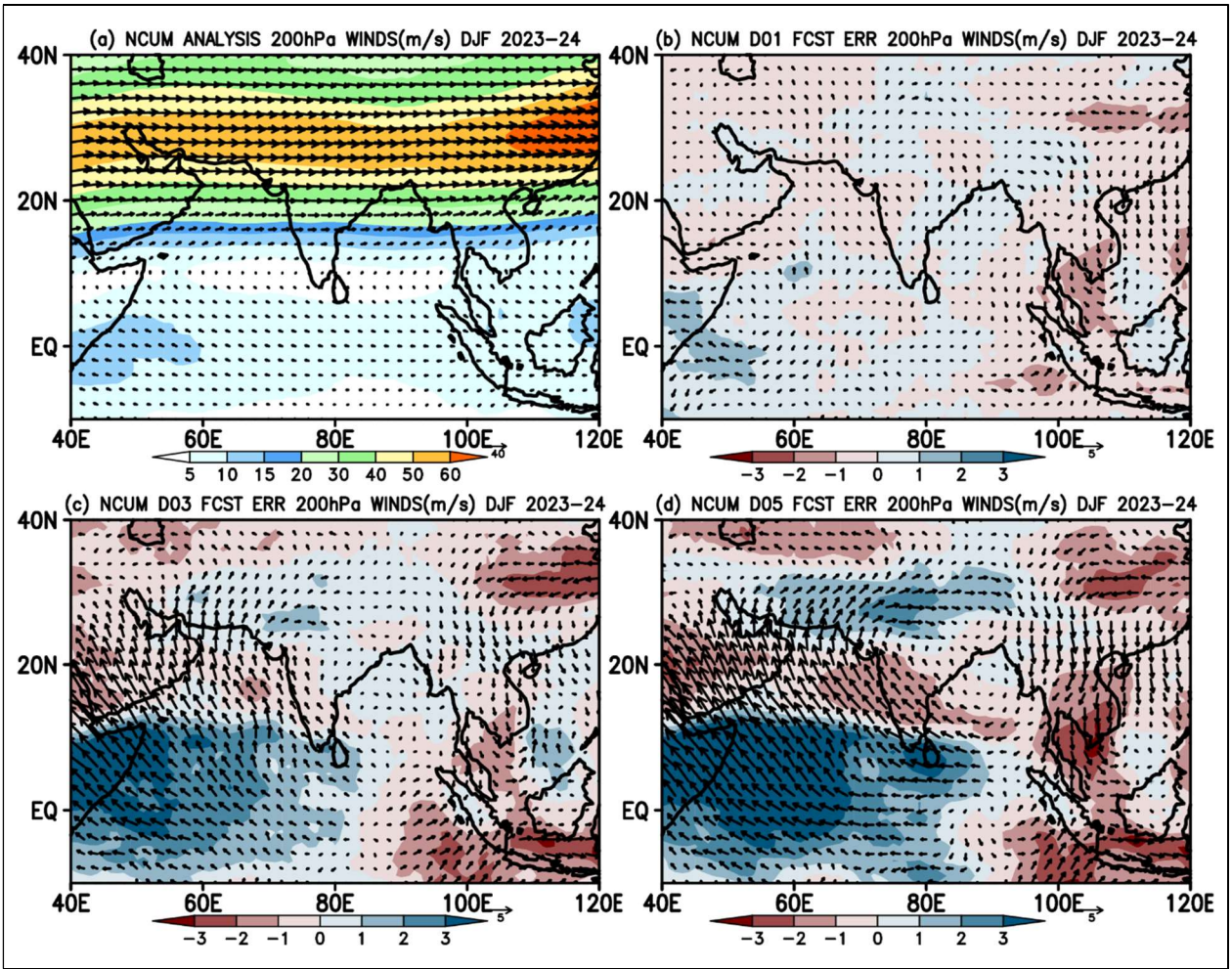

Figure 10. (a) Mean winds and systematic errors (m/s) in (b) Day-1, (c) Day-3, and (d) Day-5 forecasts at 200 hPa during DJF 2023-24.

4.2. Temperature and Relative Humidity

The spatial distribution of seasonal mean temperatures at the 850 hPa level, as analyzed by the NCUM-G model and presented in Figure 11a, reveals warmer temperatures over the southern regions of India and cooler temperatures across the northern parts, extending to the adjacent oceanic areas. The model indicates a warm bias of approximately 1°C across most of India, with this discrepancy increasing as the forecast lead time extends. Notably, temperature errors at the 850 hPa level are more pronounced over eastern Africa. Similarly, at the 700 hPa level, there is evidence of a warm bias of around 0.5°C over the northern and central Indian regions. This consistent warm bias observed at both the 850 and 700 hPa levels over central India can be attributed to anti-cyclonic circulation throughout the atmospheric column and warming due to large-scale adiabatic descent, although specific data for this is not shown.

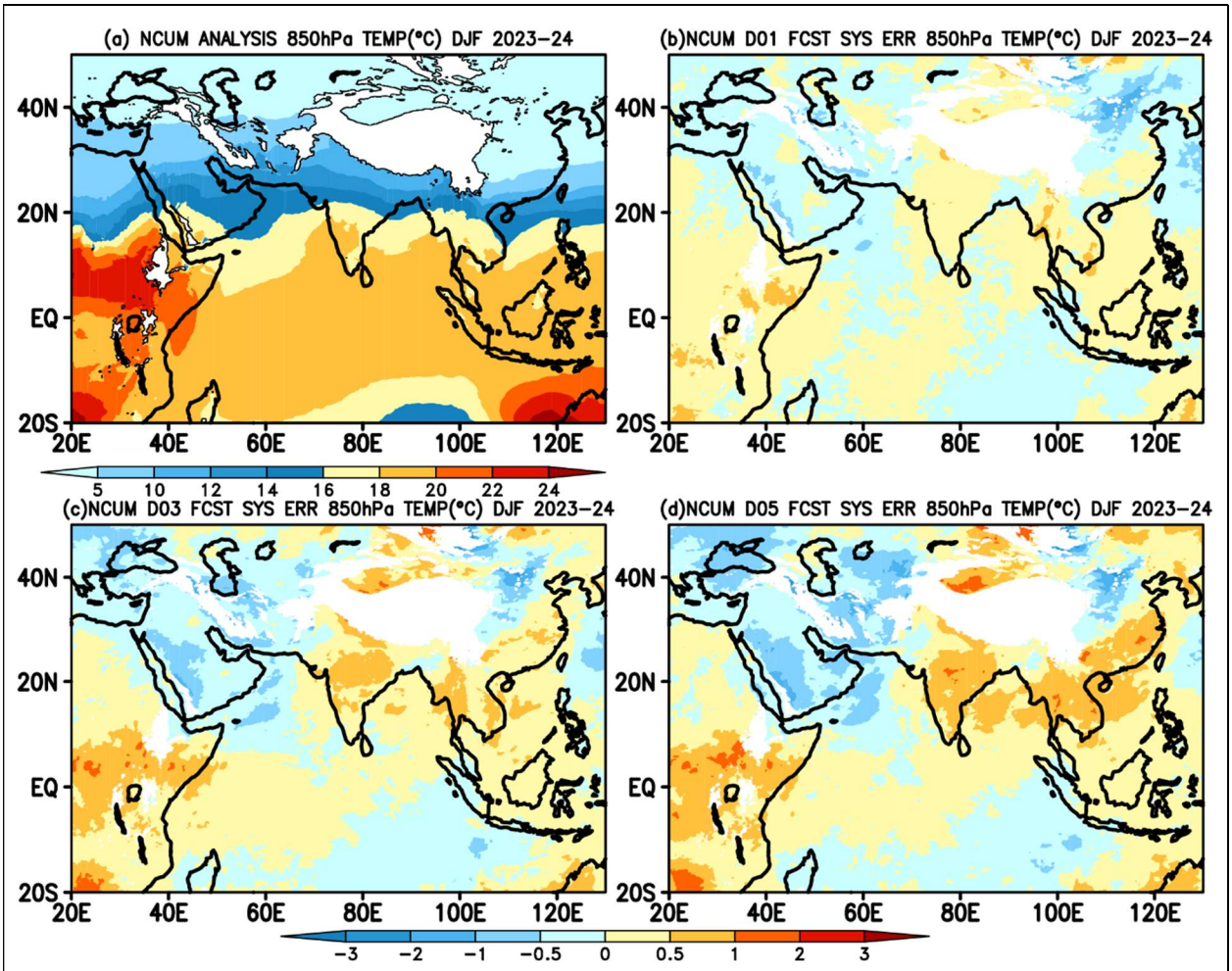

Figure 11. (a) Mean Temperature and systematic errors (Degree Celsius, ºC) in (b) Day-1, (c) Day-3, and (d) Day-5 forecasts at 850 hPa during DJF 2023-24.

Interestingly, the bias pattern reverses over 700hPa in the Bay of Bengal (BoB), showing a cold bias compared to the conditions at the 850 hPa level. This cold bias persists consistently across all forecast lead times up to Day-5, as illustrated in Figures 12c-d. Systematic errors at higher altitudes, specifically at the 500 and 200 hPa levels, exhibit warm and cold biases, respectively, over India and its surrounding oceanic regions, as seen in Figures 13c-d and Figures 14c-d. The cold bias observed over central India at the 200 hPa level may be linked to anti-cyclonic circulation, which introduces colder air from the mid-latitudes along its northern edge, as suggested by Figures 10c-d.

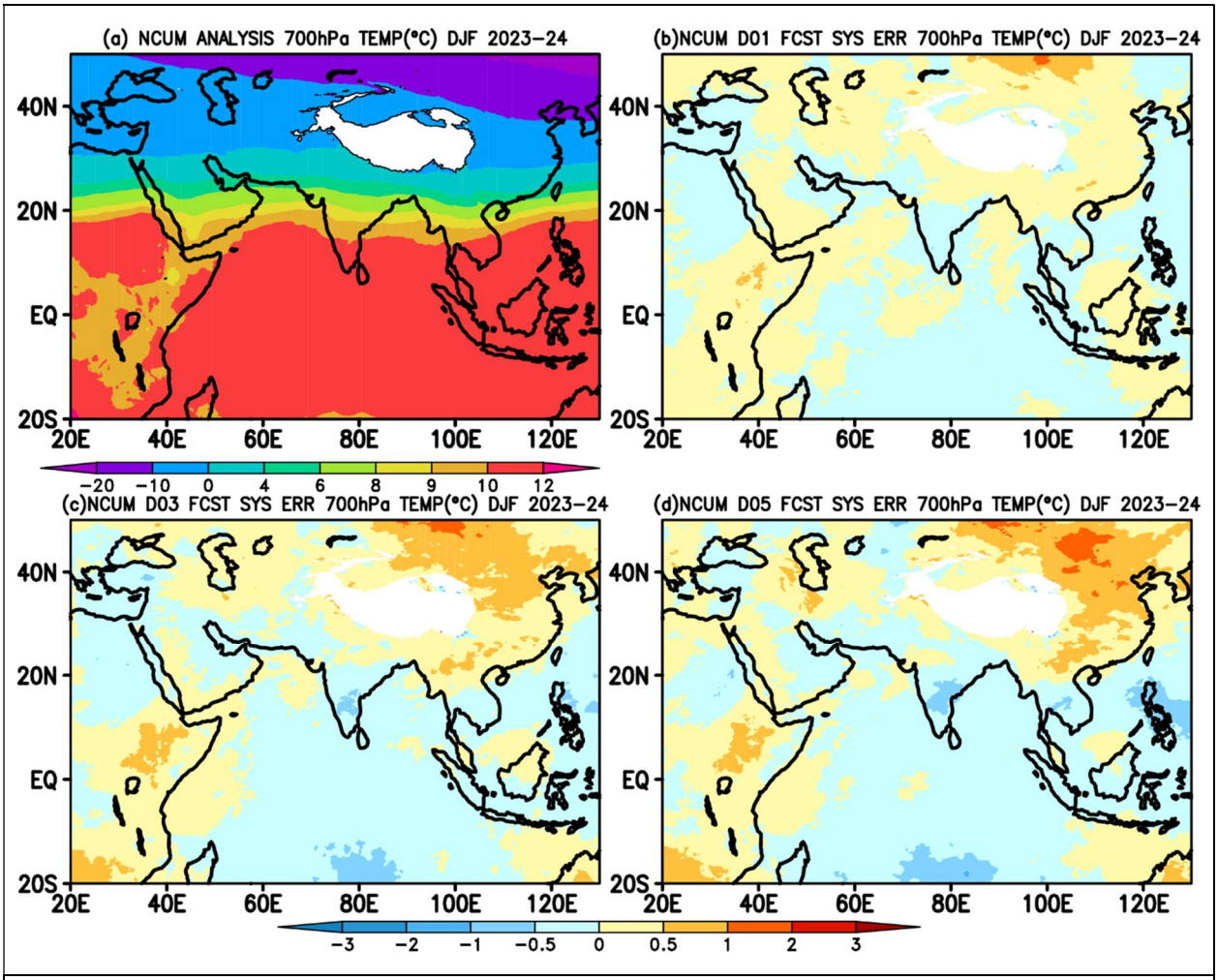

Figure 12. (a) Mean Temperature and systematic errors (Degree Celsius, °C) in (b) Day-1, (c) Day-3, and (d) Day-5 forecasts at 700 hPa during DJF 2023-24.

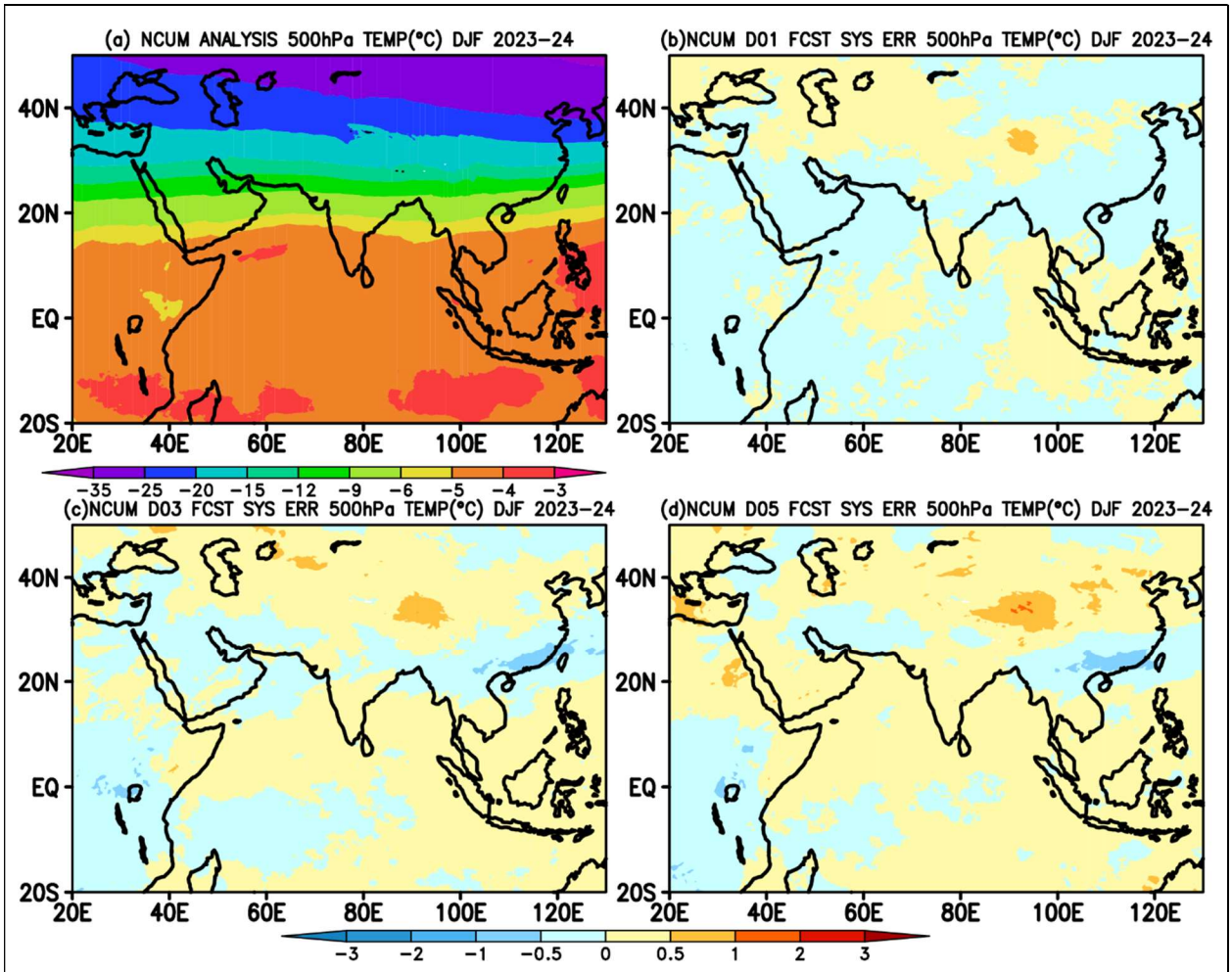

Figure 13. (a) Mean Temperature at and systematic errors (Degree Celsius, °C) in (b) Day-1, (c) Day-3, and (d) Day-5 forecasts at 500 hPa during DJF 2023-24.

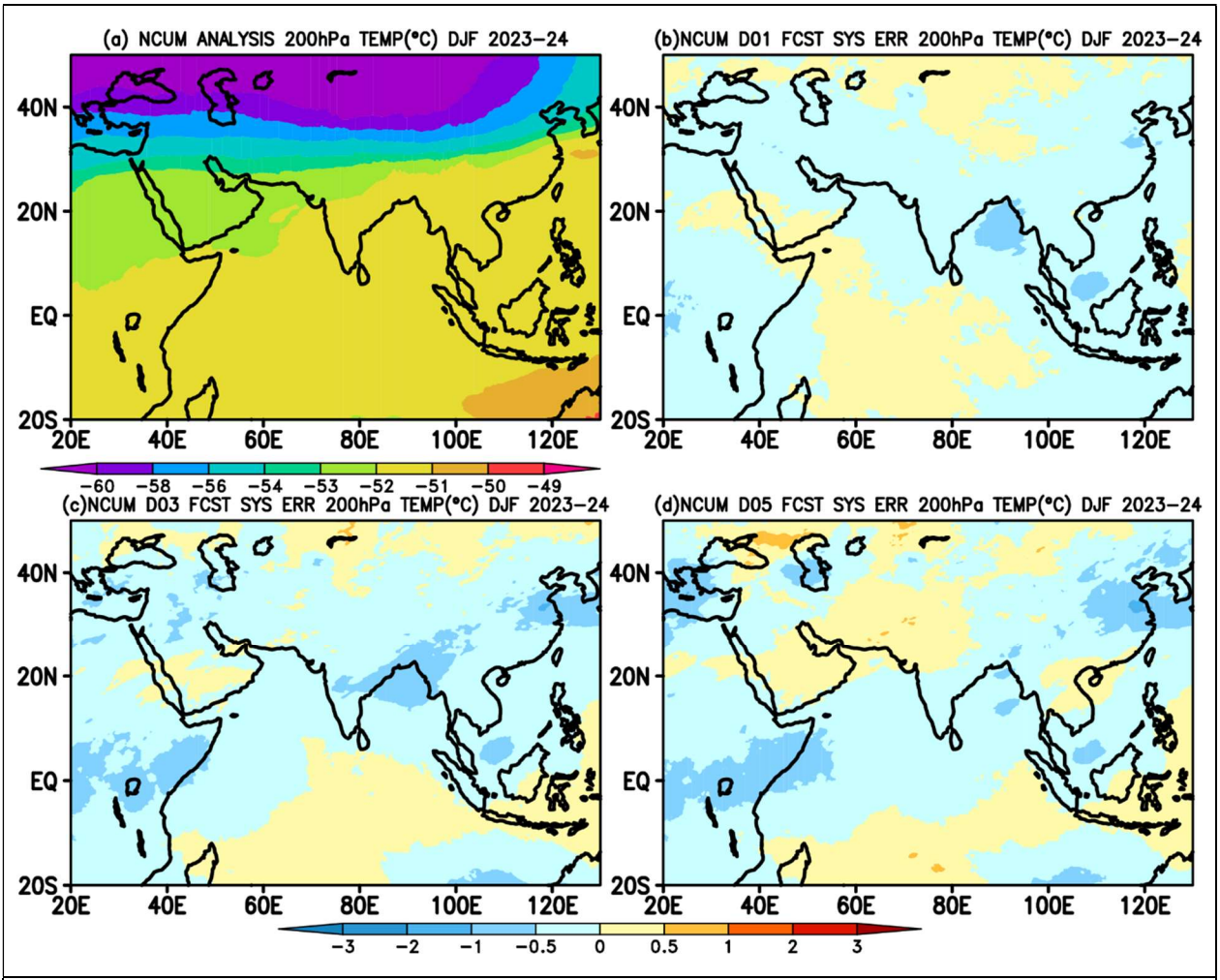

Figure 14. (a) Mean Temperature and systematic errors (Degree Celsius, °C) in (b) Day-1, (c) Day-3, and (d) Day-5 forecasts at 200 hPa during DJF 2023-24.

Seasonal mean RH at 850 hPa (Figure 15) and 700 hPa (Figure 16) levels show large values > 90% over equatorial regions and relatively lower RH values over northern parts of the Indian subcontinent. Maximum RH values are concentrated over MC. Systematic errors show a large dry bias over the Indian land regions at 850hPa level, and this dryness is enhancing with forecast lead time (Figures 15c-d). On the contrary, most of the Indian subcontinent and surrounding oceanic regions exhibit wet bias as evidenced by positive RH values, except Africa, the South China Sea, MC, and south of the equator regions. Interestingly the dry bias observed over the Indian land region at 850 hPa level change sign to positive and moist bias is seen at 700 hPa level. Additionally, the moist bias south of the equator is getting intensified in the Day-3 and Day-5 forecast and the entire column is occupied with excess moisture at 700 hPa levels (Figures 16 b-d).

In the next section, a brief description of systematic errors in the model forecasts is presented for key surface variables such as 2m Temperature (Figure 17), 10m winds (Figure 18), and Total Precipitable Water (PWAT; Figure 19). The errors are computed against the NCUM-G analysis.

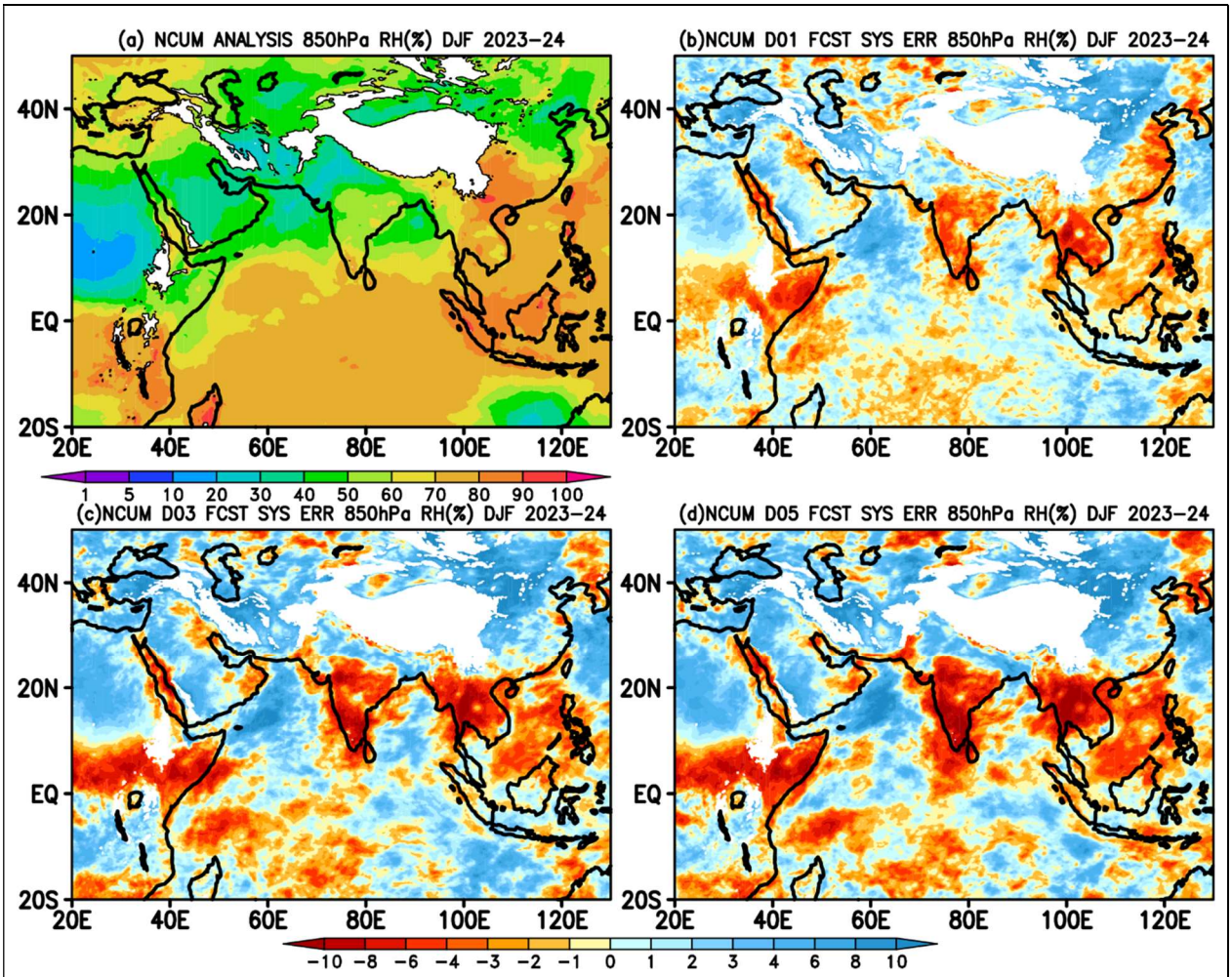

Figure 15. (a) Mean Relative Humidity and systematic errors (%) in (b) Day-1, (c) Day-3, and (d) Day-5 forecasts at 850 hPa during DJF 2023-24.

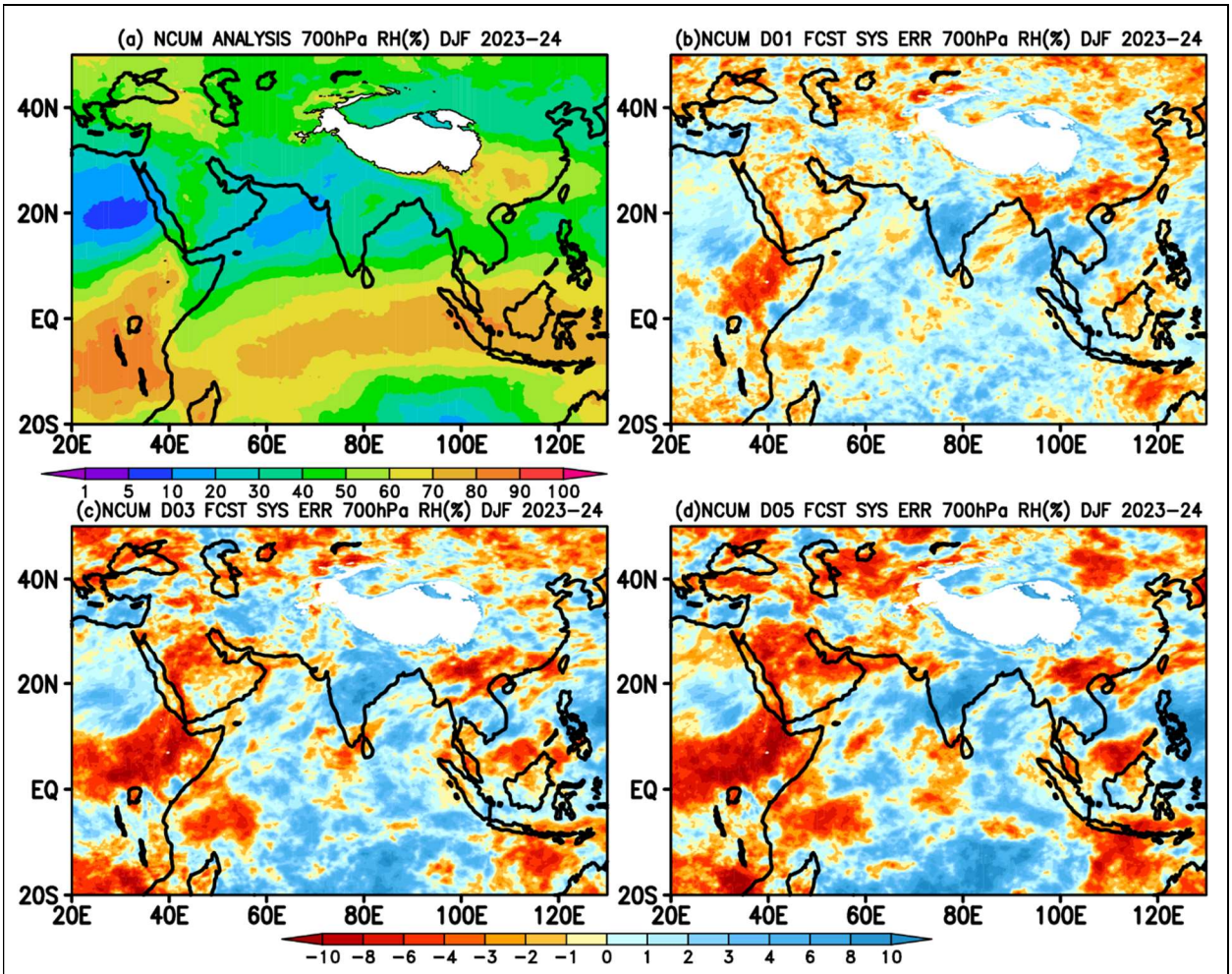

Figure 16. (a) Mean Relative Humidity and systematic errors (%) in (b) Day-1, (c) Day-3, and (d) Day-5 forecasts at 700 hPa during DJF 2023-24.

4.3. Surface (10m) winds

Seasonal mean winds at 10m from the analysis show the presence of strong North easterlies over the BoB and AS with maximum winds around open AS, the African coast, and the South China Sea. Reversal of these north easterlies to westerlies after crossing the equator is also noted in the analysis (Figure 17a). The systematic errors in the forecasts (Figures 17 b-d) depict a few notable features: 1) The North easterlies which are noticed on Day-1 (Figure 17b) changed their direction to southerlies with lead time, and it is seen on Day-5 (Figure 17d). 2) The north-westerly wind bias over northern AS in Day-1 is enhancing its strength with forecast lead time. 3) On a similar note, the easterly wind bias seen in south of the equator around ~100 ^{0}E is also getting intensified with forecast lead time (Figures 17b-d).

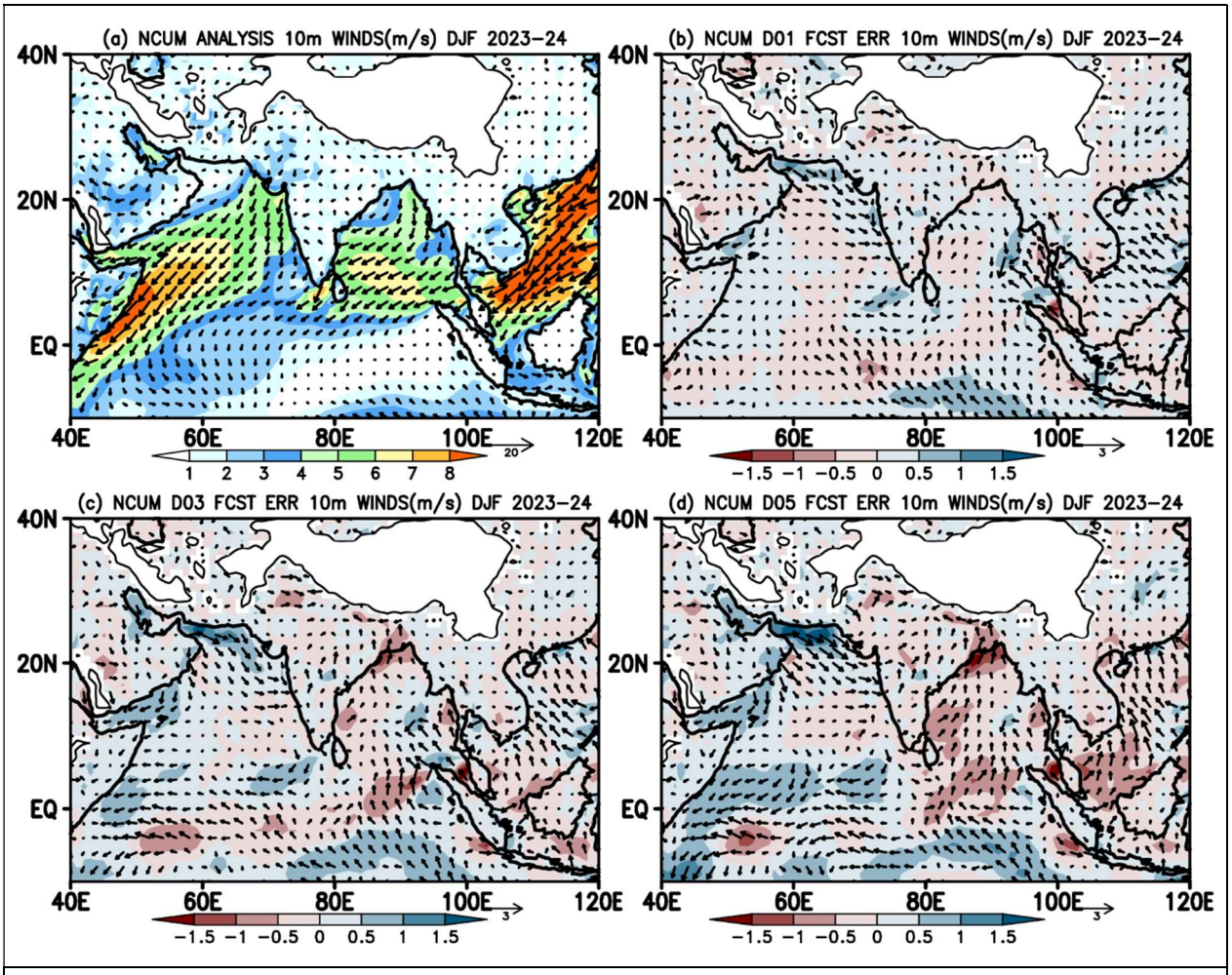

Figure 17. (a) Mean winds at 10m height and systematic errors (m/s) in (b) Day-1, (c) Day-3, and (d) Day-5 forecasts during DJF 2023-24.

4.4. Temperature at 2m

Seasonal temperature patterns over the Indian region show cold temperatures (12-15 ºC) in the north and warm temperatures (>25 ºC) towards the south (Figure 18a). Systematic errors (Figures 18 b-d) show a relatively warm bias over Indian land regions and north of 40 ºN latitude regions. Interestingly, these warm biases are increasing with forecast lead time, especially over the Indian region. This can be attributed to the dry north-westerly winds from the Northwest entering into Indian land and north AS (Figures 18 c-d). In addition, most of the oceanic regions of the BoB and AS exhibited warm bias of the range 0-0.5 ºC in all the forecast lead times.

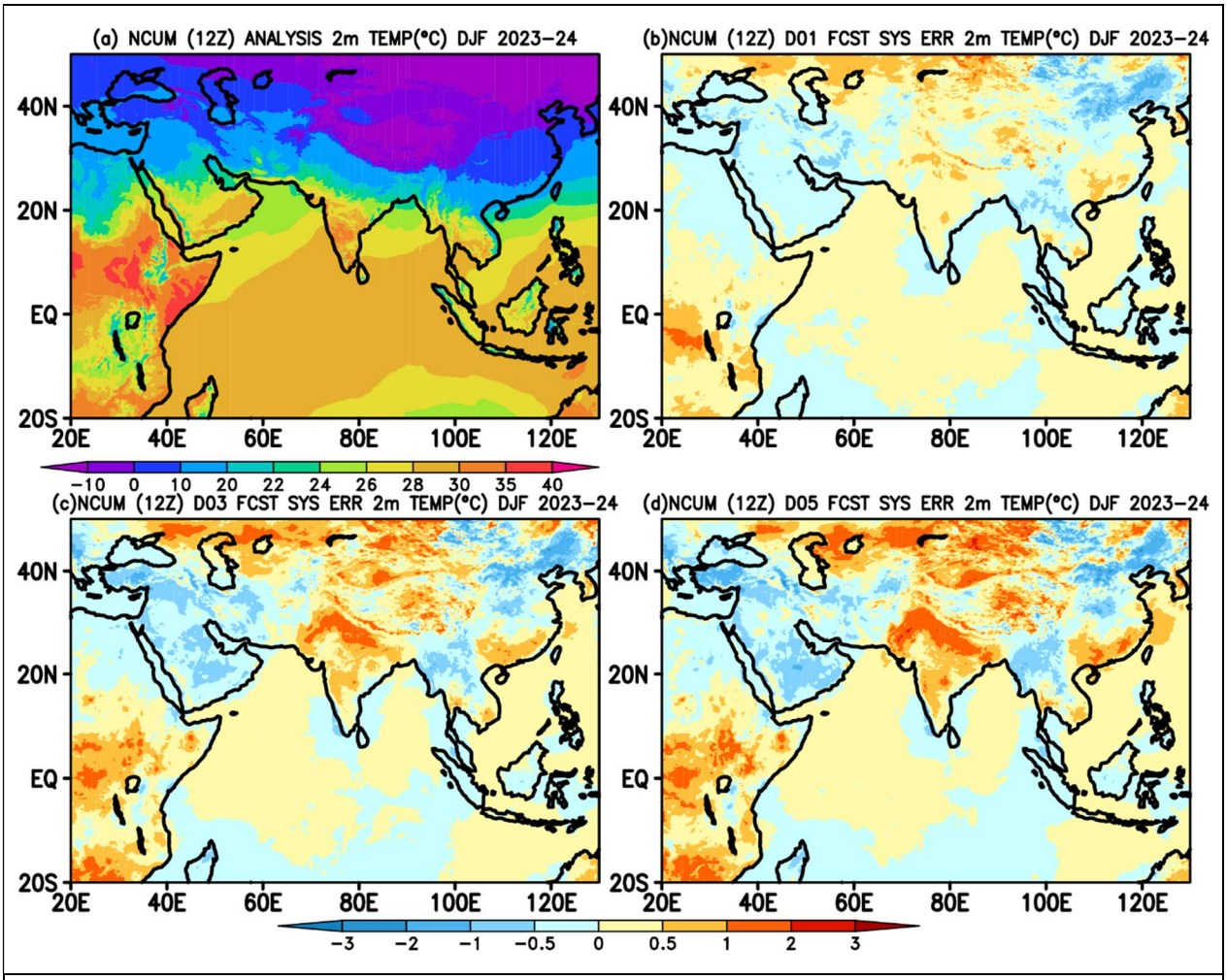

Figure 18. (a) Mean Temperature at 2m height and systematic errors (Degree Celsius, °C) in (b) Day-1, (c) Day-3, and (d) Day-5 forecasts during DJF 2023-24.

4.5. Total Precipitable Water (PWAT)

The seasonal mean PWAT displays notably high values exceeding 60 mm in the vicinity of the equatorial belt, particularly over the Maritime Continent. This phenomenon is attributed to the active phase of the Madden-Julian Oscillation (MJO) during the winter season across these areas, as highlighted in Figure 19a. Conversely, the majority of the northern and central regions of India experience arid conditions, characterized by significantly lower PWAT values ranging between 5-15 mm. An exception to this pattern is observed in the extreme southeastern peninsula of India, where moderate PWAT values around 35-40 mm prevail due to the influence of northeast monsoon conditions, also depicted in Figure 19a.

Systematic errors in PWAT forecasts, as illustrated in Figures 19b-d, indicate a tendency towards drier atmospheric columns over Indian landmasses on Day-1. This dry bias intensifies as the forecast lead time progresses, reaching its peak magnitude by Day-5, as shown in Figures 19c-d. Additionally, substantial

positive PWAT biases are evident over the Bay of Bengal (BoB), Arabian Sea (AS), and equatorial regions. The surplus column water in these areas could potentially contribute to excessive rainfall patterns observed in these regions.

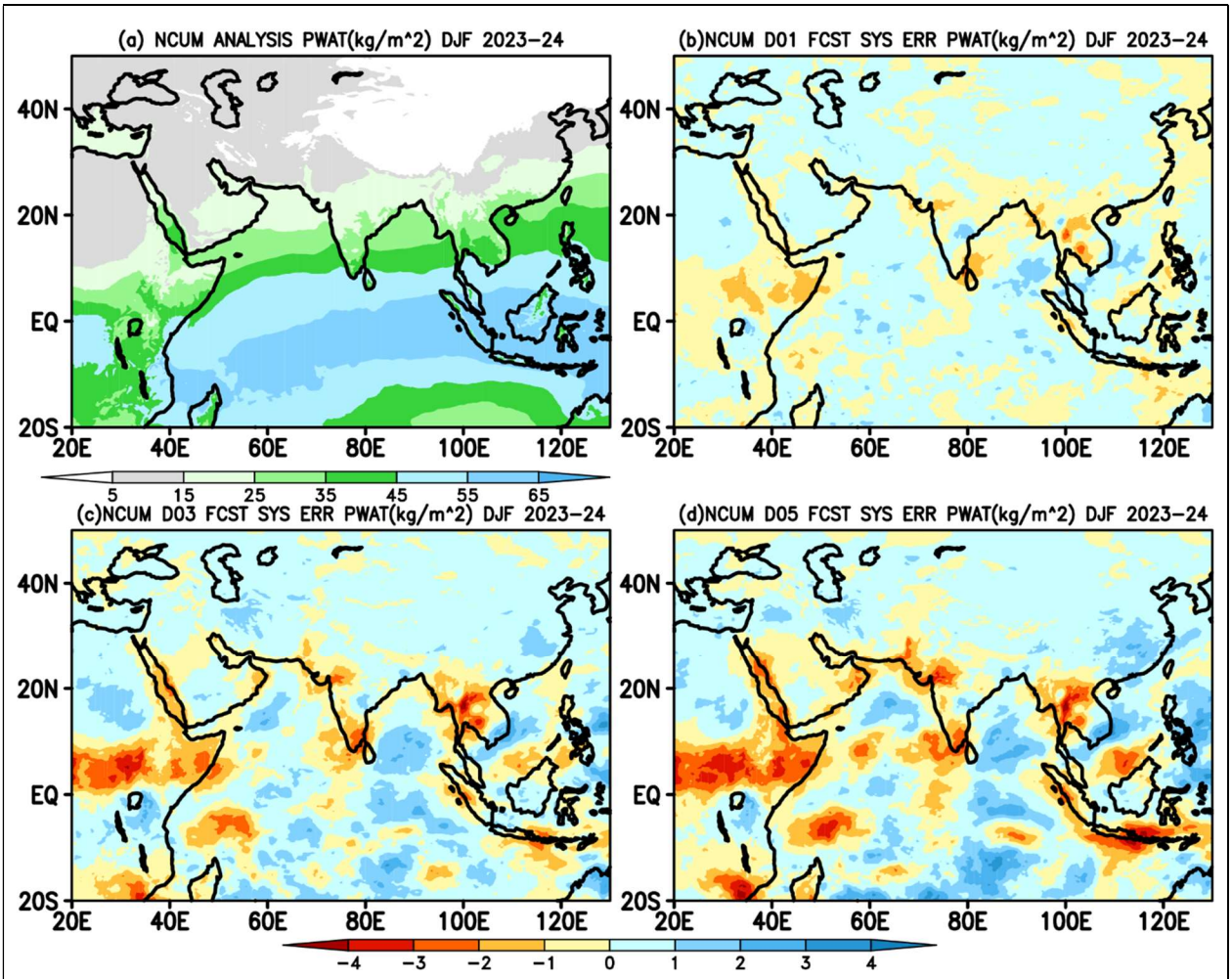

Figure 19. (a) Mean Total Precipitable Water (PWAT) up to model levels and systematic errors (mm) in (b) Day-1, (c) Day-3, and (d) Day-5 forecasts during DJF 2023-24.

5. Forecast Verification during DJF 2023-24

Verification of NCUM-G model rainfall forecasts is presented in this section for DJF 2023-24. The daily accumulated rainfall forecasts are verified against the NCMRWF-IMD merged Satellite and gauge rainfall product. The discussion presented in this section is confined to mean and mean error (ME) over the India region. Further, this section also quantifies forecast skill using standard verification metrics, namely, the probability of detection (POD), false alarm ratio (FAR), and critical success index (CSI) which are described in standard literature (Wilks, 2011, Jolliffe and Stephenson, 2012); and Symmetric extremal dependence index (SEDI), a metric for extreme and rare events (Stephenson et al 2008, Ashrit et al 2015b, Sharma et al 2021).

5.1. Rainfall Mean and Mean Error

The observed and forecasted mean rainfall during DJF 2023-24 is shown in Figure 20. Observations indicate the highest mean rainfall exceeding 8 mm/day is seen over the southern parts of peninsular India and equatorial oceanic regions. Moderate rainfall (2-4 mm/day) is seen over the Jammu and Kashmir (J & K) region, where the effect of western disturbances is more prominent, which brings a significant amount of rain to occur over these regions (Figure 20a). The panels in the middle row, Figures 20 b-d, show the Day-1, Day-3, and Day-5 NCUM-G forecast rainfall averaged during the DJF 2023-24 period. The observed peak in rainfall amount is well predicted in all the forecast lead times. However, it is found that the NCUM-G forecast overestimates rainfall amounts and spatial distribution over oceanic regions around the equator, north-eastern regions, and western parts of J & K. Apart from this, most of the Indian subcontinent is dry with no convection in both observations and forecasts. Now, to further quantification, forecast mean errors (ME) are computed against the observations. The panels in the bottom row show rainfall mean error (ME) (Figures 20 e-g) in predicted rainfall, indicating wet bias (blue) over southern parts of the oceanic regions consistent with the mean rainfall patterns (Figures 20 b-d). Small dry bias regions are noticed over Sri Lanka, western parts of south BoB, eastern parts of J & K, and some parts of Tamil Nadu in the rainfall forecasts, and the magnitude of dry bias increases with lead time (Figures 20 e-g).

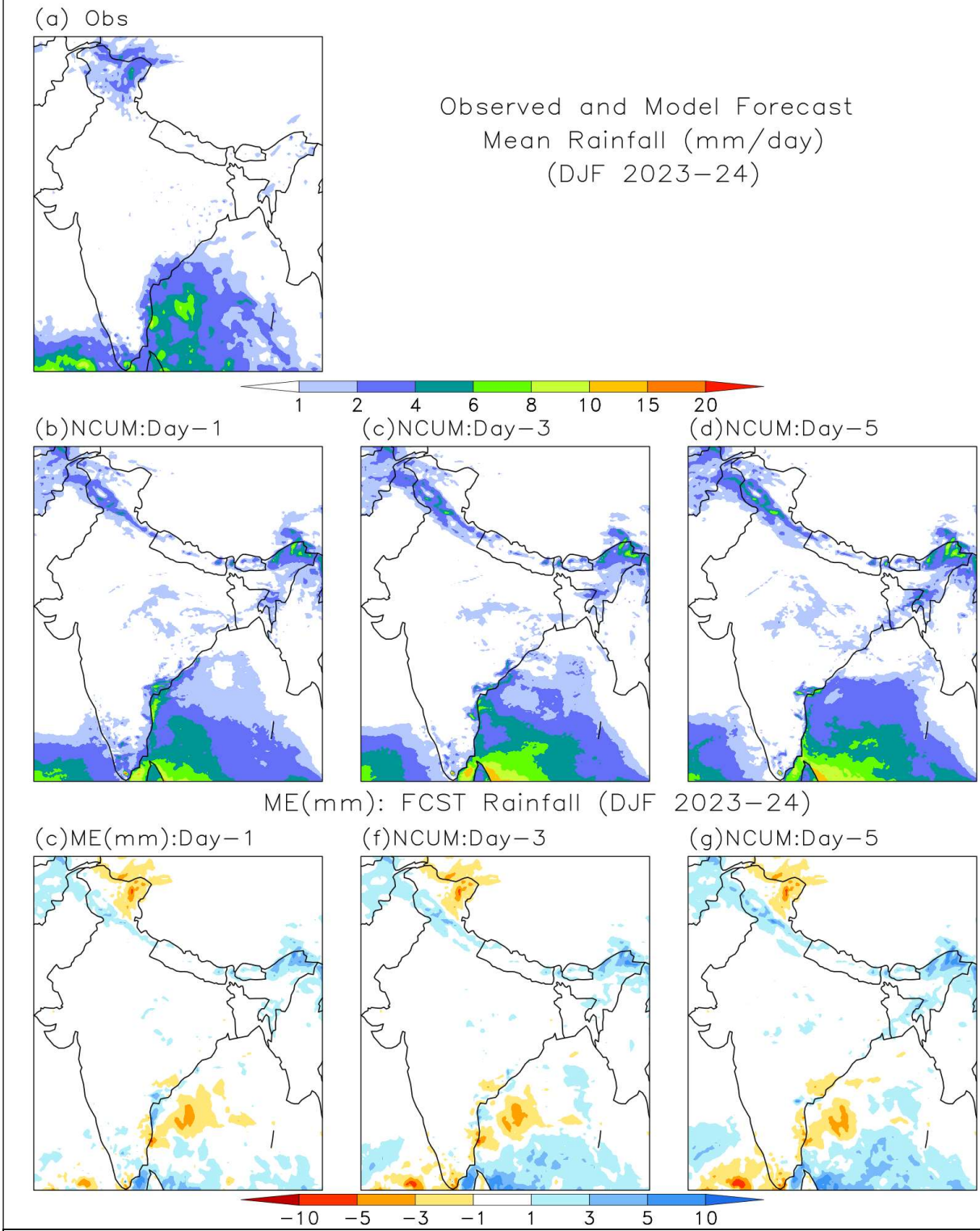

Figure 20. Accumulated DJF rainfall (mm) in (a) Observations and (b) Day-1, (c) Day-3, and (d) Day-5 forecasts. Bottom panels (e), (f), and (g) show Mean Error (ME) in Day-1, Day-3, and Day-5 forecasts, respectively.

5.2. Categorical Scores of Rainfall Forecasts

To further quantify the model rainfall forecasts, categorical skill scores are computed over the Indian subcontinent (Figure 21). The categorical approach of verifying quantitative precipitation forecast (QPF) is generally based on the 2 x 2 contingency table, which is evaluated for each threshold. Verification scores are presented for rainfall of up to 30mm/day. For different rainfall thresholds, POD and FAR show a decrease and increase in scores, respectively. The BIAS score (frequency bias) indicates that forecasts overestimate the frequency at various thresholds. The values of Peirce's skill score (PSS) and SEDI, all are high for rainfall up to 3-5 mm/day, suggesting reasonable skill. PSS score shows a very sharp decrease as the threshold varies. Overall, the skill is not bias-free. For higher rainfall thresholds (> 10 mm/day), frequency bias is almost constant, but the skill is low, as indicated by CSI, PSS, and SEDI (Figure 21).

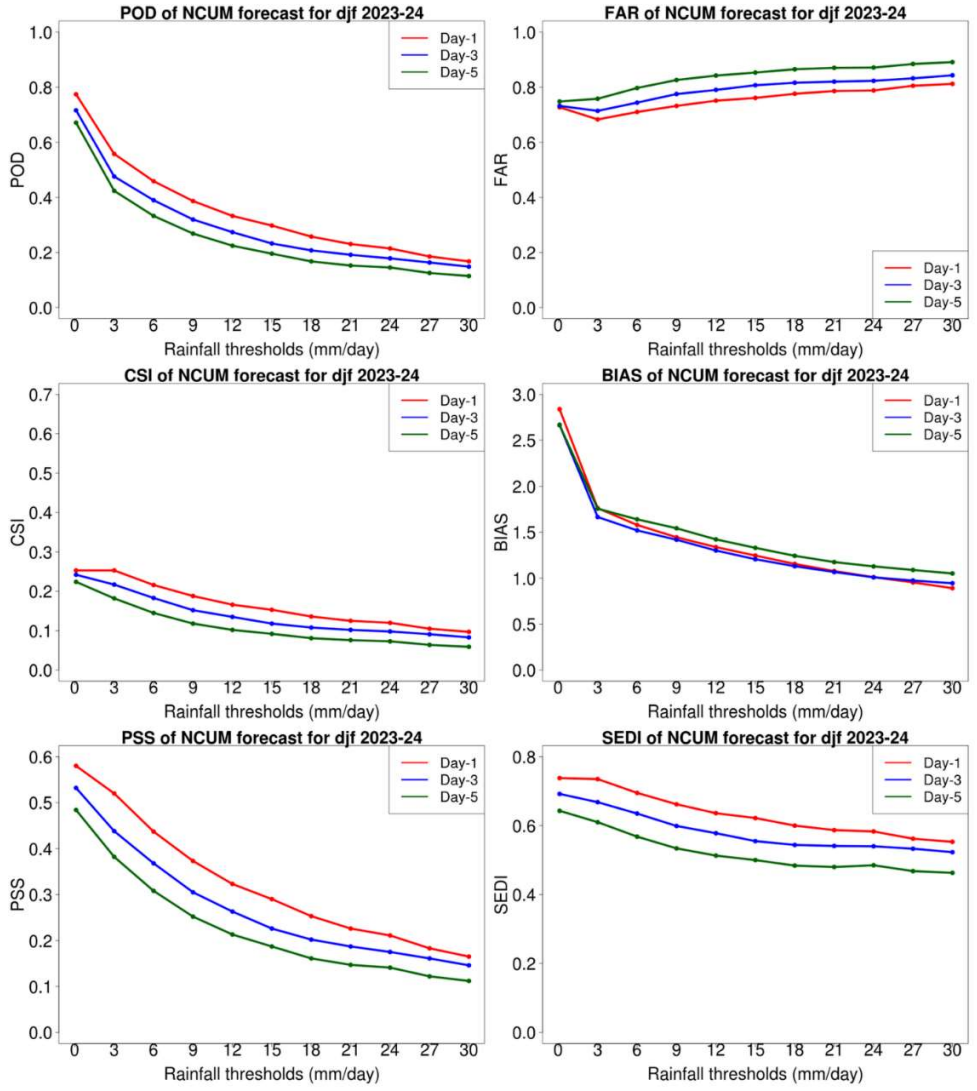

Figure 21. Categorical all India Rainfall scores POD (*top left*), FAR (*top right*), CSI (*middle left*), BIAS (*middle right*), PSS (*bottom left*), and SEDI (*bottom right*).

5.3. Categorical Scores of T_{min}

A similar analysis, as discussed in above section 5.2, is repeated for minimum temperature (T_{min}) thresholds. Interestingly the POD and PSS scores for Tmin thresholds remain nearly constant up to 20-22 ºC with values less than 0.4. However, the PSS scores slightly increase at 22-24 ºC (Figure 22). FAR scores over India as a whole show relatively large values >0.6 up to temperature thresholds 20-22 ºC; later a gradual decrease is noticed in all the forecast times (Figure 22).

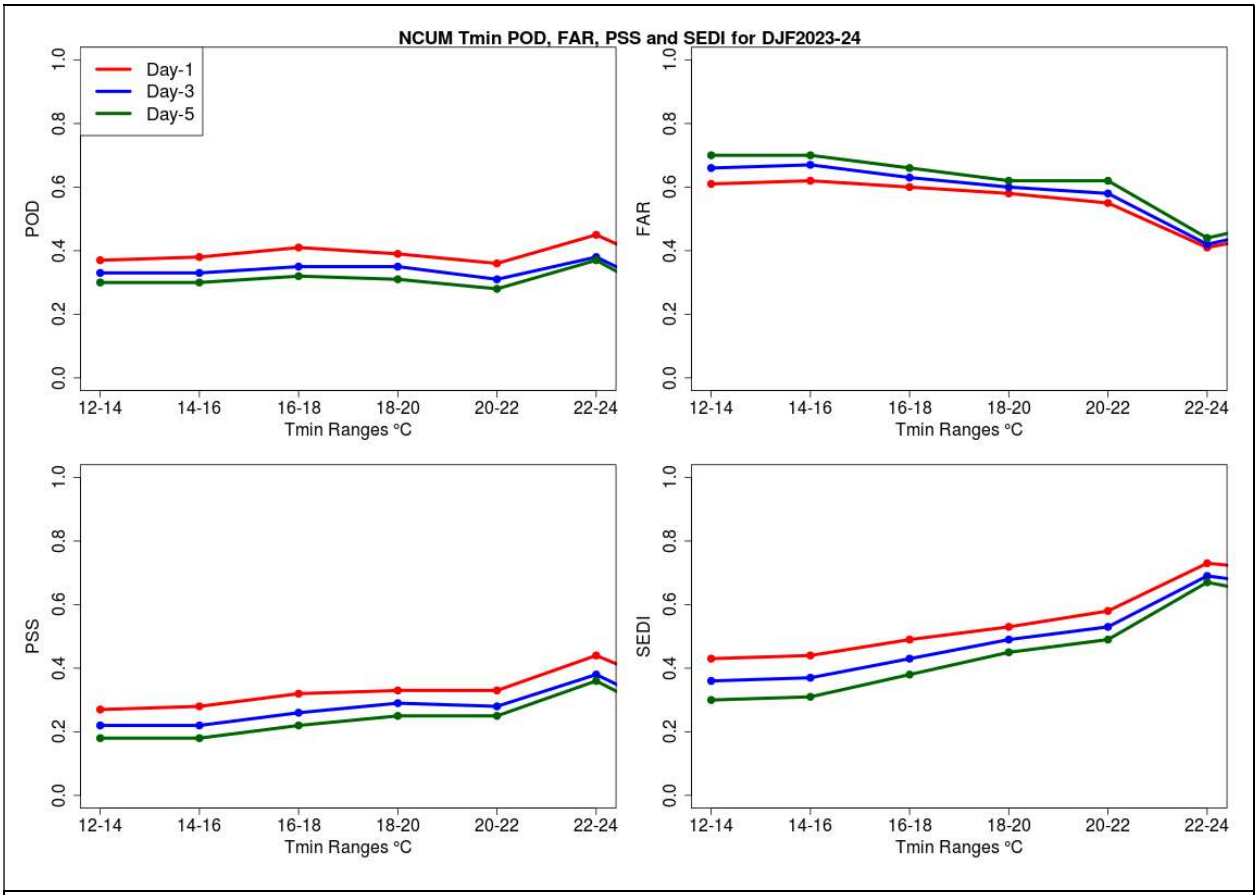

Figure 22. Categorical all India T_{min} scores POD (*top left*), FAR (*top right*), PSS (*bottom left*), and SEDI (*bottom right*).

6. Significant Weather Events during DJF 2023-24

This section summarizes the significant weather events, such as the cyclones, western disturbances, cold waves, extreme rainfall events, etc., that happened during the DJF 2023-24 season, along with the forecast assessment from the NCUM-G model.

6.1. Bay of Bengal Severe Cyclonic Storm (SCS) "Michaung" during 01-06 Dec 2023

This section gives a summary report on the verification of the NCMRWF model forecasts for the recent Severe Cyclonic Storm (SCS) 'MICHAUNG' during 01-06 Dec 2023, which developed over the BoB and crossed the coast between Nellore and Machilipatnam (lat lon would be better) between 07-09 UTC of 5th May 2023. Verification of forecast tracks and intensity is presented for all NCMRWF Unified Models; NCUM-G (12 km grid resolution), NCMRWF Global Ensemble Prediction System (NEPS-G; 12 km grid resolution), and NCMRWF Regional Unified Model (NCUM-R; 4 km grid resolution) for both 00UTC and 12UTC runs. Forecast tracks and verification are presented for model-predicted tracks against IMD best track data. Appendix-1 gives details of all NCMRWF models and forecasts used for tropical cyclone forecasting.

6.1.1. Forecast Tracks and Strike Probability

The observed and predicted tracks based on 00UTC of 1st Dec 2023 are shown in Figure 23 (top). All the predicted tracks indicated that the SCS "Michaung" would track towards Andhra Pradesh (AP) coasts. The strike probability (Figure 23; bottom) based on the 23 (1 control+22 perturbed)-member NEPS-G ensemble indicates that the cyclone would approach the coast of AP/Tamil Nadu (TN). The forecast track errors are discussed in the next section.

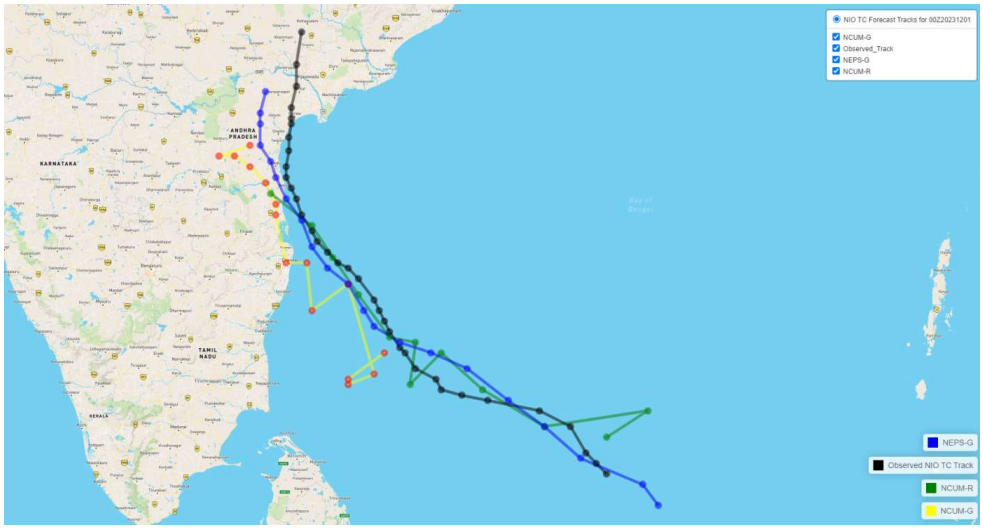

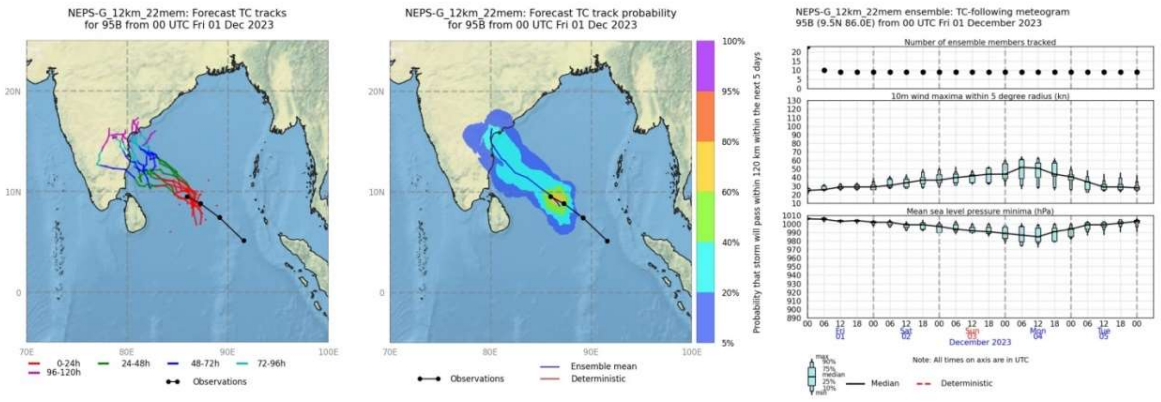

Figure 23. Observed & forecast tracks of Bay of Bengal SCS 'Michaung'. Forecast tracks, strike probability, and EPS grams are based on IC 00UTC 1st Dec 2023.

6.1.2. Forecast Track Errors

The NCUM-G, NCUM-R, and NEPS-G (ICs from 29 Nov - 05 Dec 2023) tracks based on 00UTC and 12UTC runs have been used in the verification. Table 1 summarizes the track errors at different lead times. The mean initial position error is the least (32 km) in NCUM-G, while it is highest in NCUM-R (73 km). NCUM-G and NEPS-G have Direct Position Error (DPE) < 100 km (200 km) up to 60 h (120 h).

The track error components of Direct Position Error (DPE), Along Track Error (ATE), and Cross Track Error (CTE) are shown in Figure 24. DPE, ATE & CTE are highest in NCUM-R up to 72hrs. NEPS-G forecasts show mean CTEs are less than 100 km at all the lead times.

Table 1. Forecast Track Errors NCUM-R, NCUM-G, and NEPS-G (numbers in the adjacent column in italics indicate the number of forecast points validated)

	DPE					
Fcst Hour	**NCUM-R**	**No of Fcst verified**	**NCUM-G**	**No of Fcst verified**	**NEPS-G**	**No of Fcst verified**
0	73	*6*	32	*5*	35	*10*
12	96	*9*	43	*6*	43	*11*
24	102	*9*	55	*6*	43	*10*
36	116	*8*	71	*8*	54	*9*
48	160	*10*	61	*8*	65	*8*
60	155	*11*	69	*7*	82	*7*
72	219	*10*	119	*8*	83	*6*
84			130	*9*	81	*5*
96			152	*8*	69	*4*
108			152	*7*	98	*3*
120			174	*6*	185	*2*

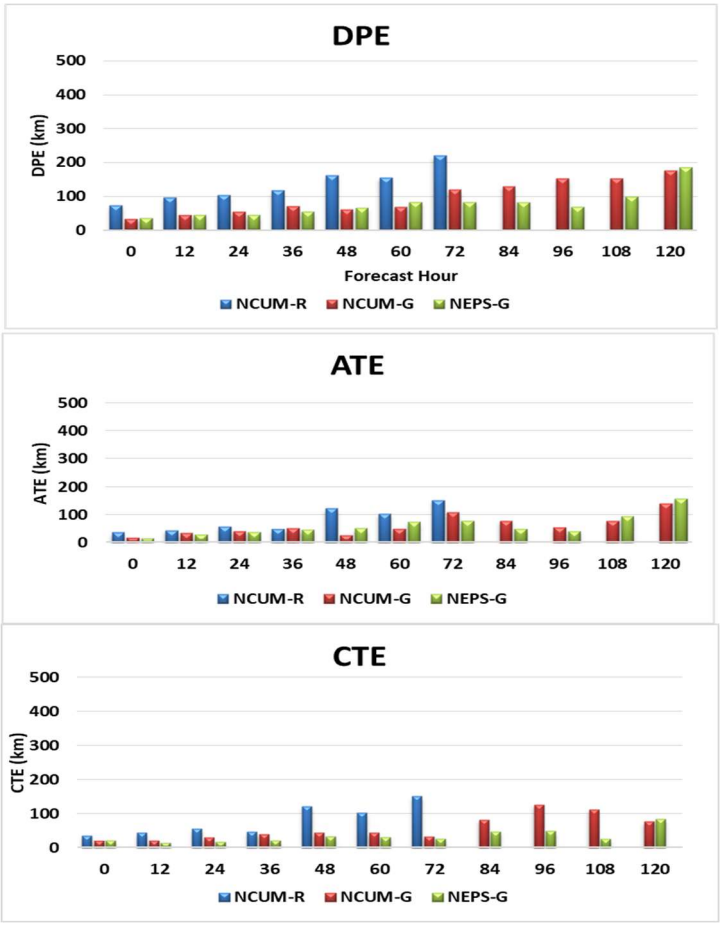

Figure 24. Track forecast errors (top) Direct Position Error (DPE), (middle) Along Track Error (ATE), and (bottom) Cross Track Error (CTE) in km.

6.1.3. Forecast Intensity errors (Min SLP and Max Wind)

The mean absolute error (MAE) in forecast central pressure (CP)/minimum Sea level Pressure (Min SLP) and maximum sustained wind (MSW) for NCUM-R and NCUM-G models is shown in Figure 25. The average error in CP is low in NCUM-R after 12 hr forecasts. At the initial time, the MEA in CP and MSW is < 10 (hPa and kt, respectively) in both NCUM-G & NCUM-R. The CP forecasts from both models are relatively better, with MAEs being less across all forecast hours. The MAE in MSW is lower in NCUM-G up to 72 hrs, but NCUM-G shows higher errors in MSW beyond 72 hrs. Model intensities for different initial conditions (IC) are presented in Figure 26. NCUM-R has a better representation of intensity after 1st Dec, whereas NCUM-G shows an underestimation tendency for all the ICs except 4th Dec.

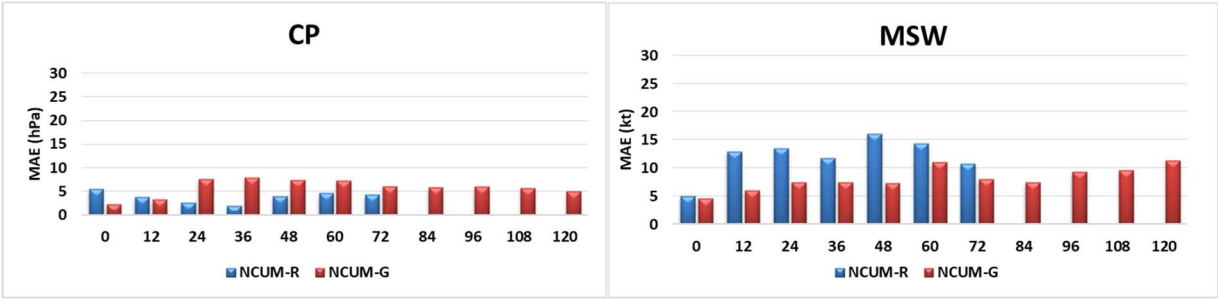

Figure 25. Mean Absolute Error (MEA) in CP (hPa) and MSW (kt) at different forecast lead times.

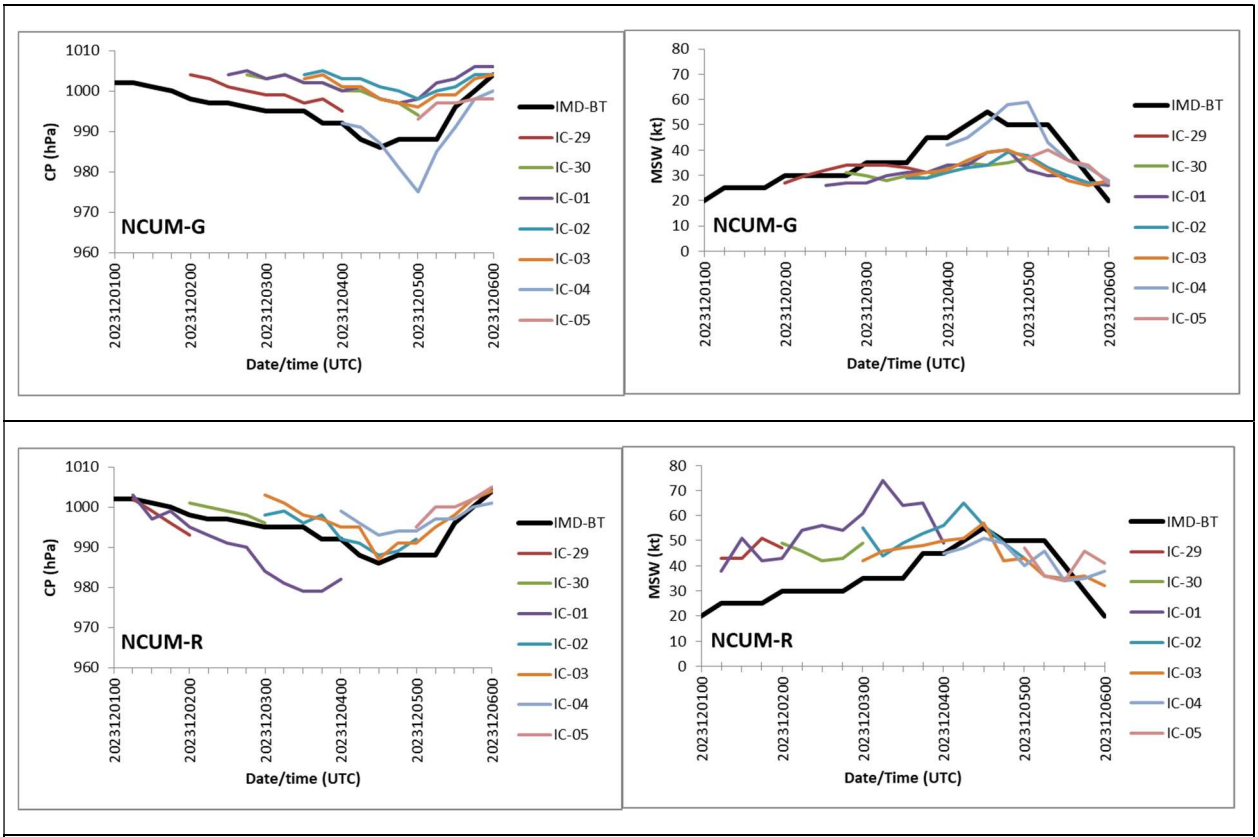

Figure 26. Intensity is given by MSW (left) & Min SLP (right) in NCUM-G (top) and NCUM-R (bottom) forecasts with different initial conditions.

6.1.4. Forecast Landfall Error

As per the IMD, the best track data for the SCS "Michaung" landfall time is between 07-09 UTC on 5th Dec, and the position is 15.7 ºN and 80.3 ºE over the coasts of AP. The forecast landfall errors have been computed using the first forecast position on the land and the previous position from the model. The forecast landfall position and time errors are tabulated in Table 2. The position of TC landfall prediction was more accurate in NEPS-G having the landfall errors less than 50 km from the model IC of 2nd Dec. The errors are below 50 km in both the global models from 12 UTC of 2nd Dec. The landfall time errors are relatively lower in NCUM-G, but NEPS-G predicted the landfall time more accurately on 12UTC of 3rd and 00 UTC of 4th Dec run with almost zero errors.

Table 2. Error in the forecast landfall time and position (Forecast time – Observed time) [-ve depicts early landfall and +ve shows delay in landfall]

	NCUM-G		NCUM-R		NEPS-G	
	Position	**Time**	**Position**	**Time**	**Position**	**Time**
2023120100	262	-24	133	-30	97	-9
2023120112	50	-6	45	-18	175	-24
2023120200	105	-3	45	-12	32	-3
2023120212	50	-3	50	-6	35	12
2023120300	35	-3	30	-6	34	9
2023120312	45	-3	67	-6	26	0
2023120400	45	-6	80	6	13	0

6.1.5. Verification of Strike Probability

Cyclone strike probability is the probability of locating a cyclone within 120 km of any grid point (see Figure 24; bottom panel). Verification of strike probability is presented using Relative Operating Characteristics (ROC) and Reliability diagrams (attributes diagrams). It must be noted that the verification of strike probability is presented for a common period from 1-5 Dec 2023. The Reliability diagram gives a comparison of forecast probability against the observed frequencies. A perfect match will show all points along the diagonal line. Points above the diagonal suggest underestimation (lower forecast probabilities), while points below the diagonal suggest overestimation (higher forecast probabilities).

For the SCS "Michaung" case, the strike probability verification obtained from NEPS-G is carried out using the best track data. Figure 27 shows the reliability (left) and ROC (right) plots for the strike probability verification. In the Reliability diagram, the points along the diagonal would indicate the best-performing model. While points below (*above*) would indicate over (*under*) estimation of cyclone strike probability. *The ROC curves of NEPS-G show that the models have the skill* as the curves are away from the diagonal line of no resolution. The AROC (area under the ROC) is 0.84, which is also indicative of good resolution in the model.

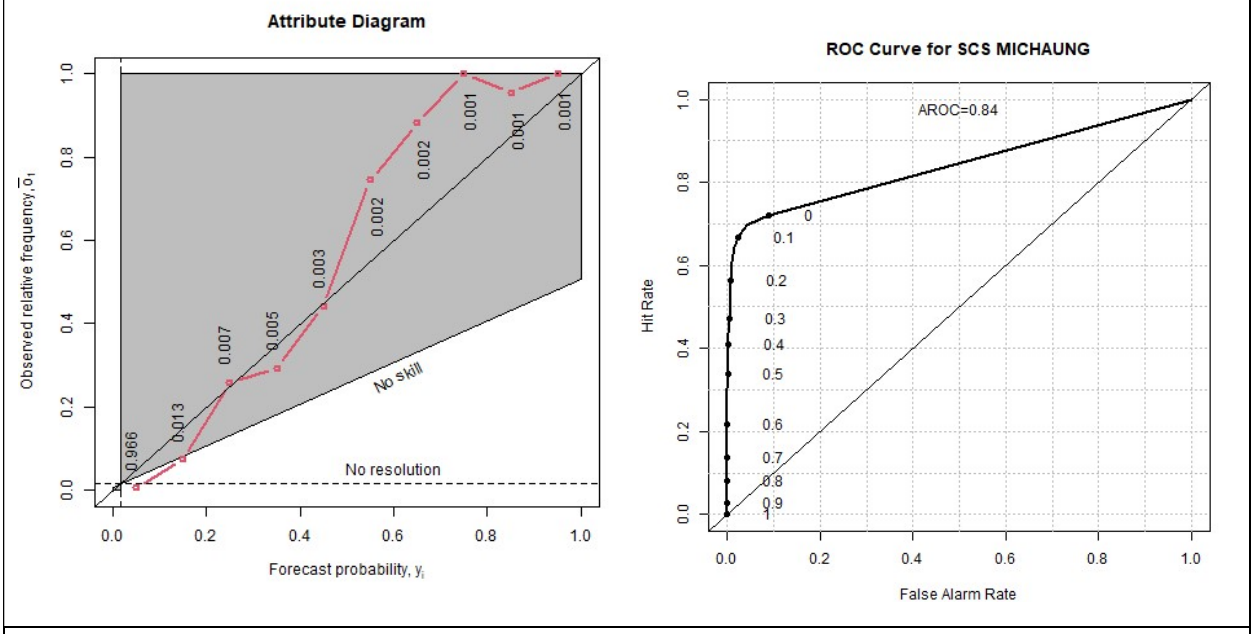

Figure 27. Verification of strike probability using reliability diagram (left) and ROC curve (right) for the case of SCS 'Michaung'.

6.1.6. CRA Verification of Rainfall Forecasts

Contiguous rain areas (CRA) verification is a spatial verification method (Ebert and Gallus, 2009) that focuses on individual weather systems and verifies the properties of the forecast objects, which allows the estimation of location error of the forecast entity. Detailed description of the method with the application over India can be found for UM Rainfall forecasts over India (Ashrit et al., 2015a) and MoES Models (NCUM & GFS) in Sharma et al., (2020). Here, NCUM-G rainfall forecasts corresponding to the SCS 'Michaung' on 4th and 6th Dec 2023 are discussed briefly using CRA verification (Figures 28 a-d). The results are presented for Day-3 (left panels) and Day-5 (right panels) forecasts valid on 4th Dec 2023 (top) and 6th Dec 2023 (bottom). On 4th Dec 2023, prior to the landfall, the cyclone was near the coast; observed rainfall is mainly confined to the Sea, including the eastern coast of India. The forecasts underestimate all attributes '*grid points>40mm*' (i.e., spatial coverage), '*Average Rainfall*', '*Maximum Rain*', and '*Rain volume*'. In the Day-3 forecast, the 40mm/day object is shifted by 0.5^o eastwards and 0.8^o northwards, while the Day-5 forecast object is shifted by 1.5^o westwards and 0^o northwards. Contribution to RMSE from pattern error is dominating (48.96% in Day-3 and 65.09% in Day-5 forecasts). On the other hand, the observed rainfall on 6th Dec 2023 (Figures 28 c,d), covers parts of Andhra Pradesh, Chhattisgarh, Telangana, and Odisha. The forecasts overestimate all the attributes. In this case, the results are presented for the 20mm/day CRA threshold. In the Day-3 forecast, the 20mm/day object is shifted by 0.5^o eastwards and 1^o northwards, and in the Day-5 forecast, the object is shifted by 1.2^o

eastwards and 1.5° northwards. The contribution to RMSE is, again, mainly from the pattern error (72.33% in Day-3 and 59.62% in Day-5).

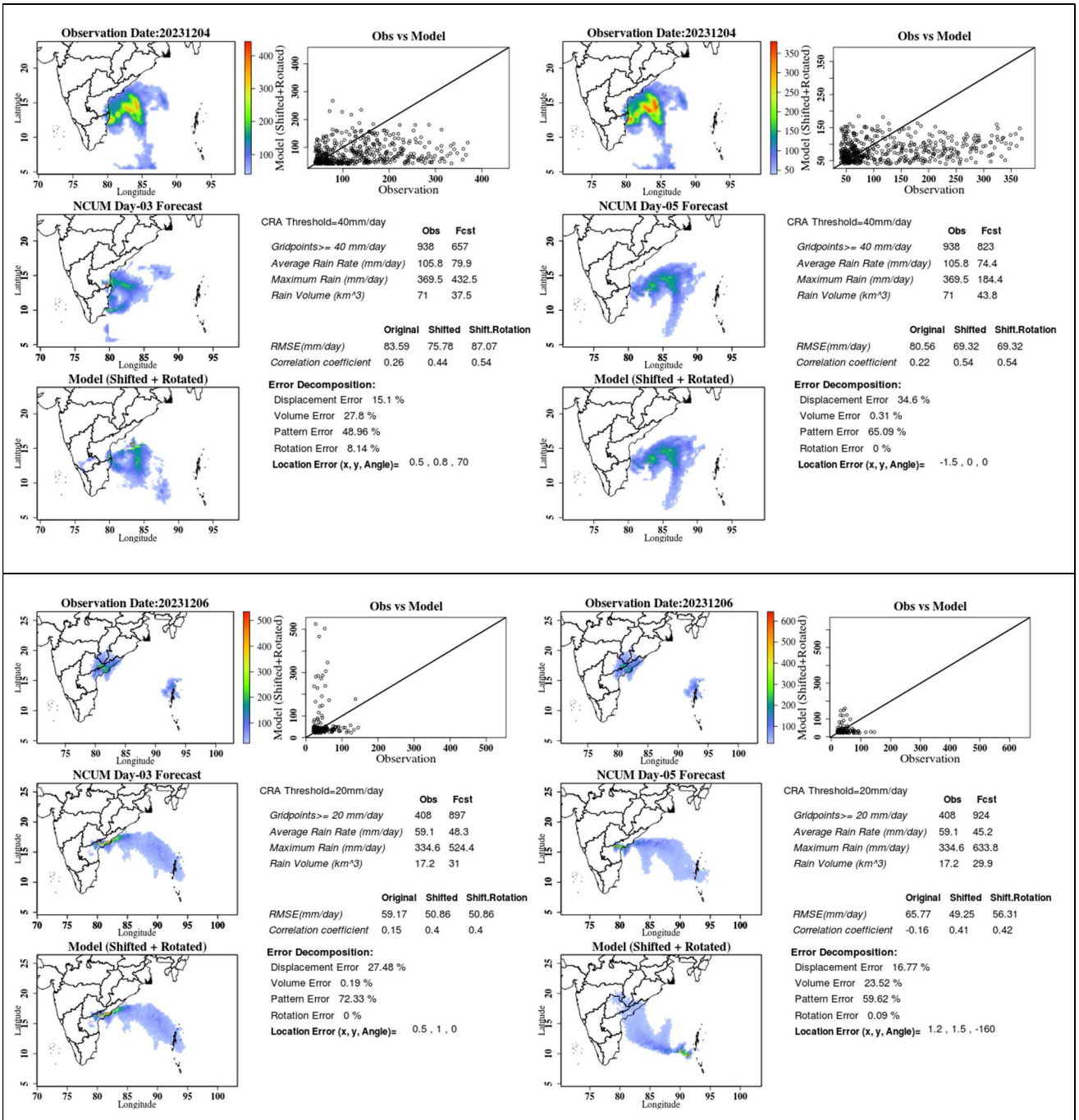

Figure 28 CRA verification of (a) Day-3 and (b) Day-5 rainfall forecasts valid on 4th Dec 2023 for 40 mm/day threshold. Similarly, CRA verification of (c) Day-3 and (d) Day-5 forecasts valid on 6th Dec 2023 is presented for the 20 mm/day threshold.

6.2. Cold Waves & Western Disturbance (WD)

6.2.1. Verification of Tmin & Western disturbance

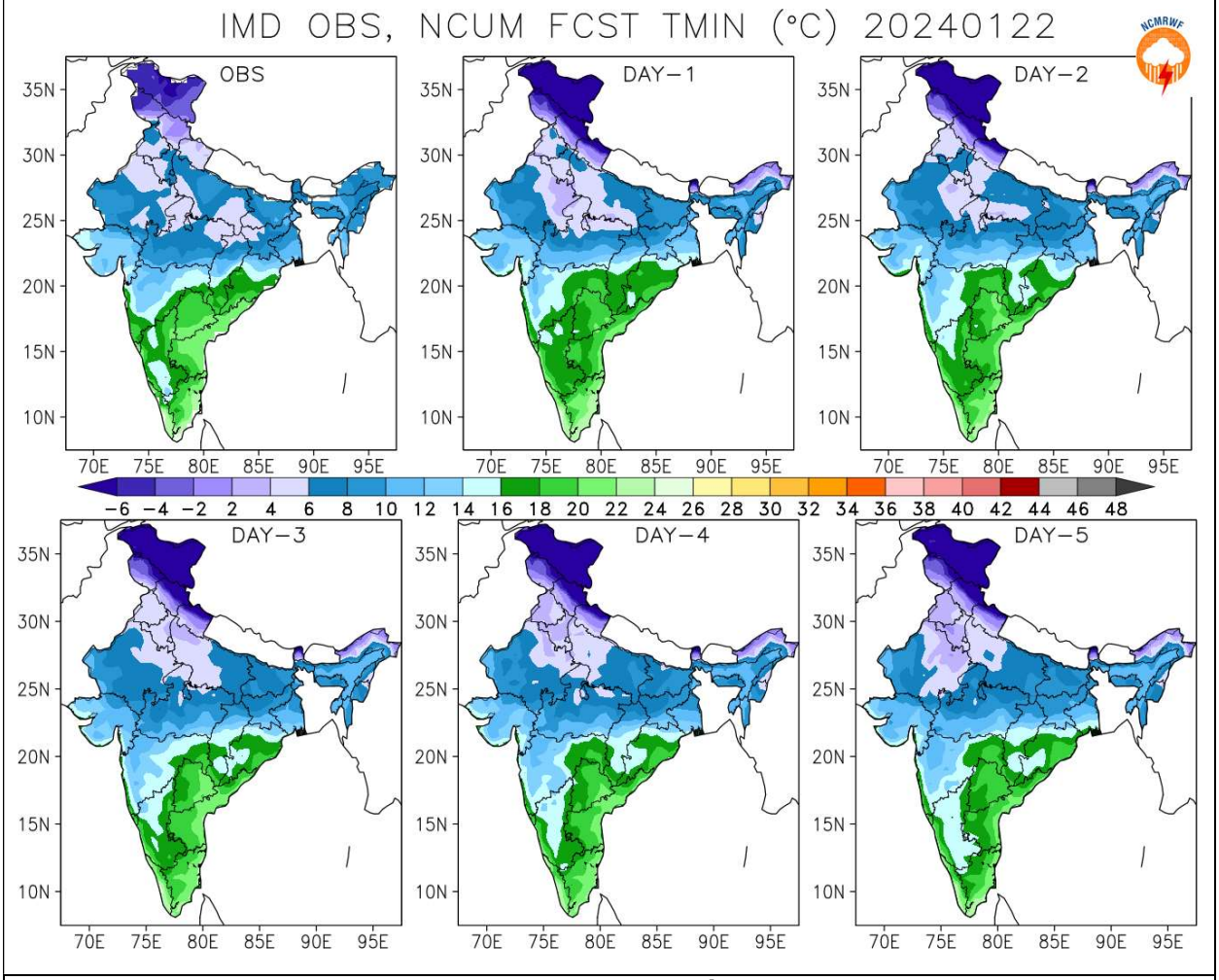

Figure 29. Observed and forecast Tmin valid on 22nd Jan 2024 over India.

Figures 29 and 30 show the observed and forecast minimum temperature on 22nd Jan 2024 and 25th Jan 2024, respectively. A large part of north India shows Tmin lower than 100C in the observations, which is accurately predicted in each of the forecasts. A minimum temperature of < 60 C is seen in the observations over northwest India (see Figure 29). The NCUM-G forecasts successfully predict the low Tmin values over northwest India. However, the model forecasts show low temperatures over a larger area. Similarly, Figure 30 shows the observed and forecast Tmin on 25th Jan 2024. The forecasts show a reasonable match with the observations. Out of all the WDs during the winter season (DJF), 2023-2024, listed in Table 3, we have chosen the strongest WD case for this report. The NCUM-G model forecasts clearly indicate the location and intensity of the trough

and WD formation as seen in observation (see Figure 31) and associated rainfall over northwestern India (see Figure 32).

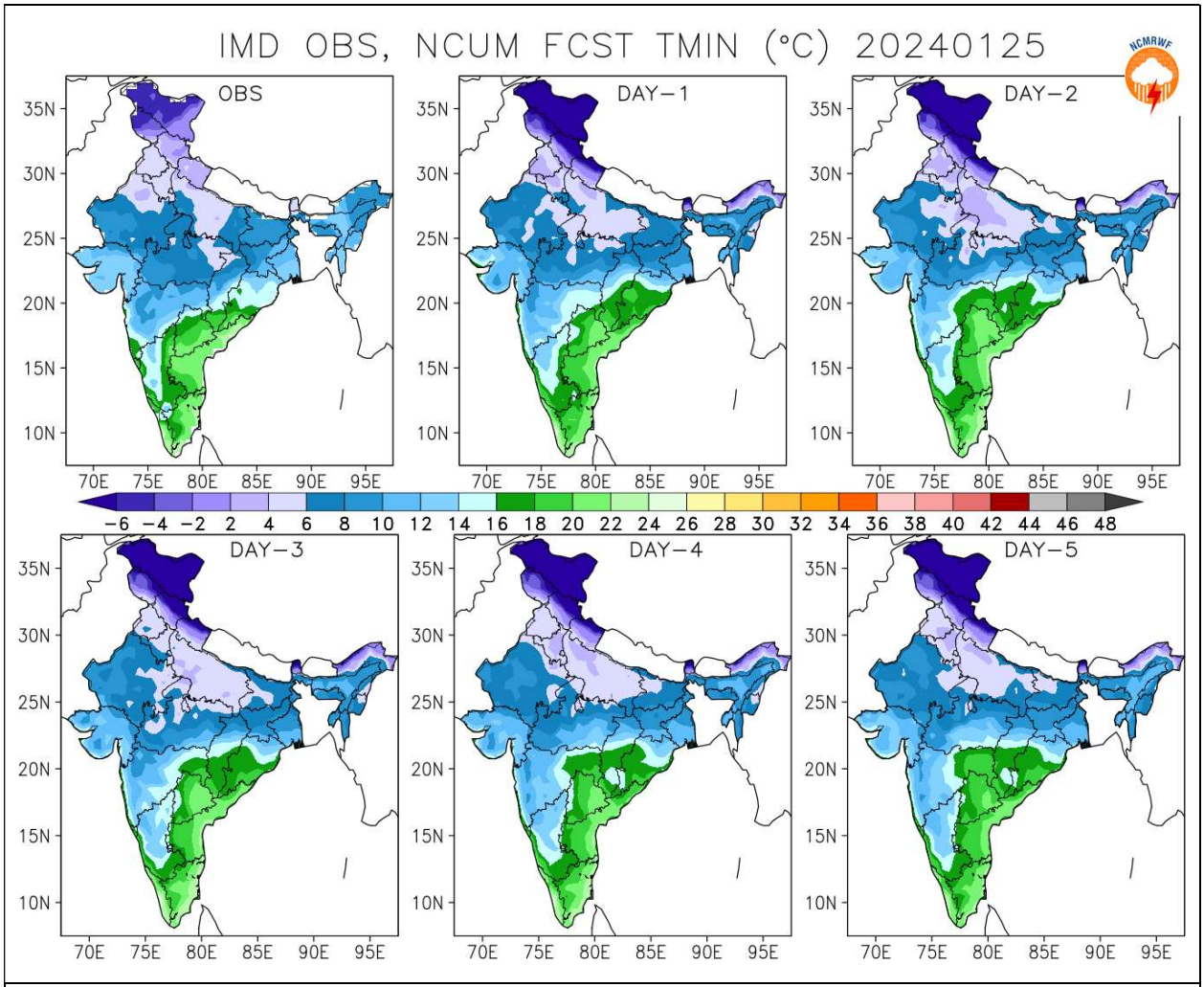

Figure 30. Observed and forecast Tmin valid on 25th Jan 2024 over India.

Table 3. List of DJF seasonal Western Disturbances.

S. No.	Month	Western Disturbances (WDs)
1.	December	There was **below-normal WD** activity over Northwest India.
2.	January	**4 WDs** (i.e., 3-8 Jan, 7-11 Jan, 25-27 Jan and 28-31 Jan)
3.	February	**8 WDs** (i.e., 30 Jan-2 Feb, 3-8 Feb, 12-19 Feb, 18-22 Feb, 22-24 Feb, 23-27 Feb, 26-28 Feb, and 28 Feb.-1 March)

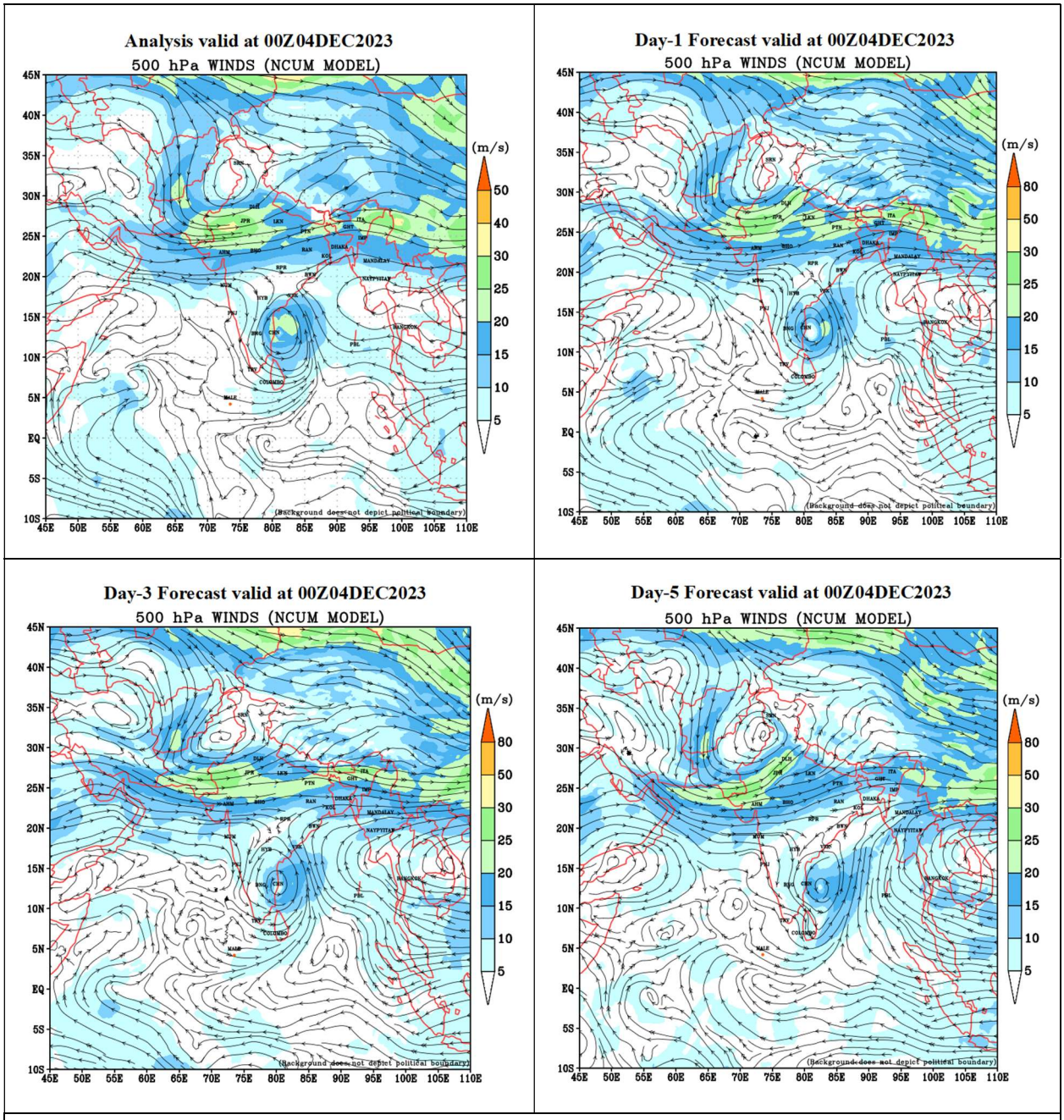

Figure 31. NCUM-G winds at 500 hPa in the analysis and Day-1, Day-3, and Day-5 forecasts valid on 4th Dec 2023.

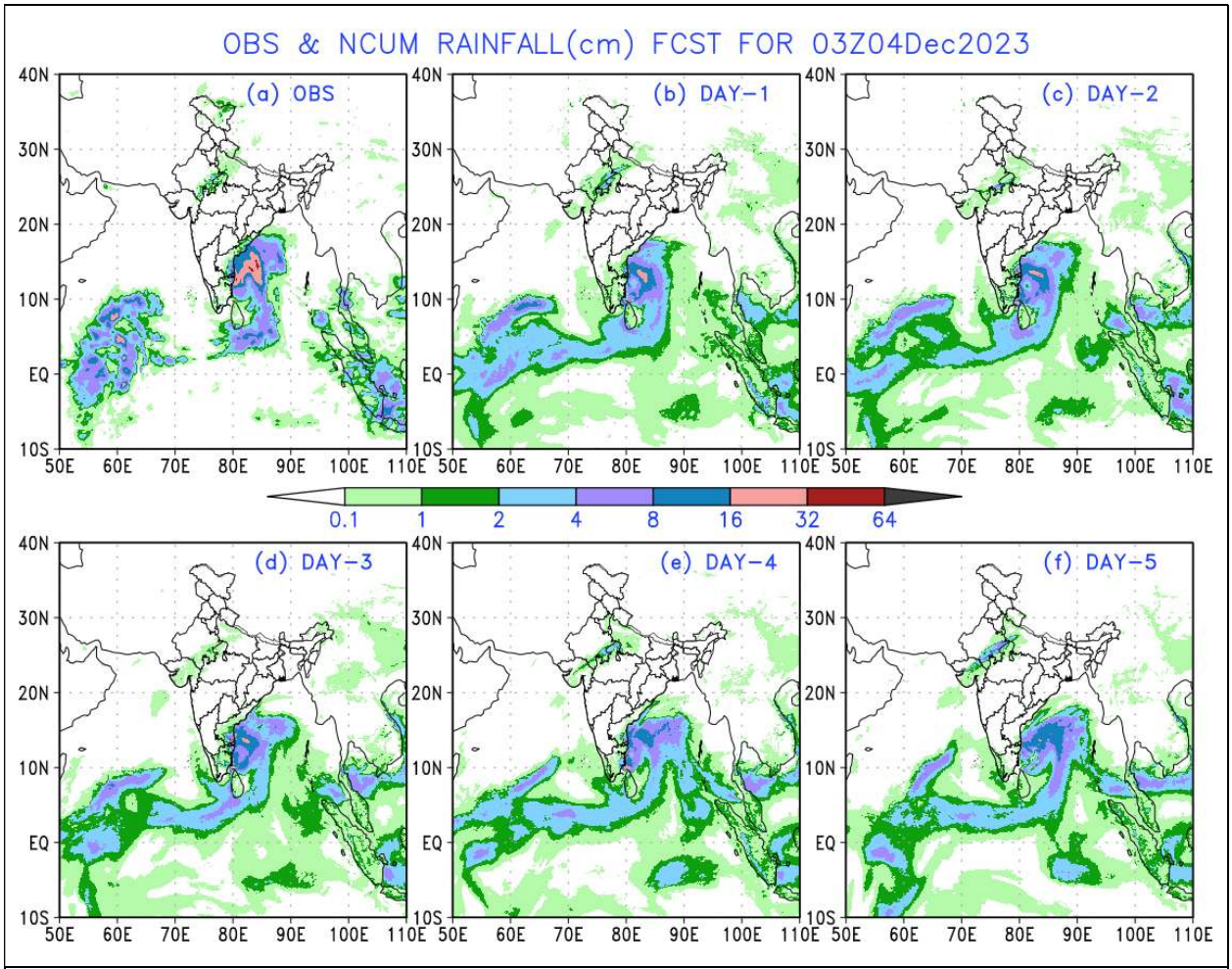

Figure 32. Observed and forecast Rainfall valid on 4th Dec 2023.

6.2.2. Observed and forecasted daily Tmin time series

Further, verification of the Tmin forecasts based on the NEPS-G ensemble is shown for several locations over northwestern India. Observed Tmin data is obtained from SYNOP stations over India via the GTS network. Figure 33 shows the forecasts with IC of 4th Dec 2023. The NEPS control (red), ensemble mean (blue), and ensemble members (green) are compared with the observations (black). Observed Tmin generally lies within the spread of ensemble members. Ensemble mean shows a very good match with the observations and successfully predicts a sharp rise/fall in value consistent with observations. The sharp drop in observed Tmin in Agra, Lucknow, Kota, and Jamshedpur by about ~9^{0}C between 08-12 (03-04) Dec 2023 is accurately predicted. Similarly, another case of cold wave in December 2023 is shown in Figure 34 for IC of 29th Dec 2023. Prolonged spell of low Tmin is indicated in the forecasts consistently. The sharp drop in observed Tmin in Jodhpur (Ambala) by about 5^{0}C (3 ^{0}C) between 31st Dec 2023- 3rd Jan 2024 (30th Dec 2023-2nd Jan 2024) is accurately predicted.

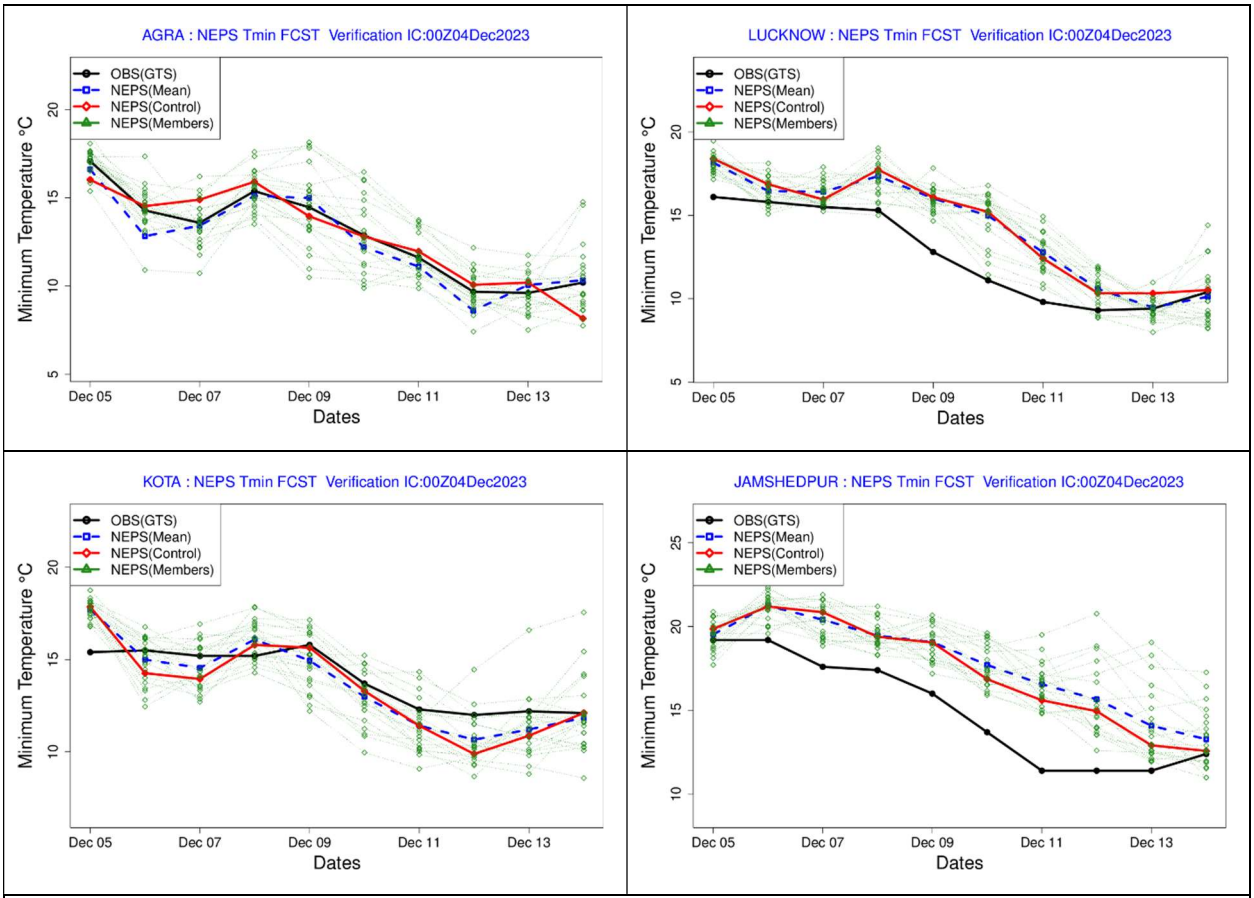

Figure 33. Observed and NEPS-G forecast Tmin over different cities in North India during the cold wave conditions of 4th Dec 2023.

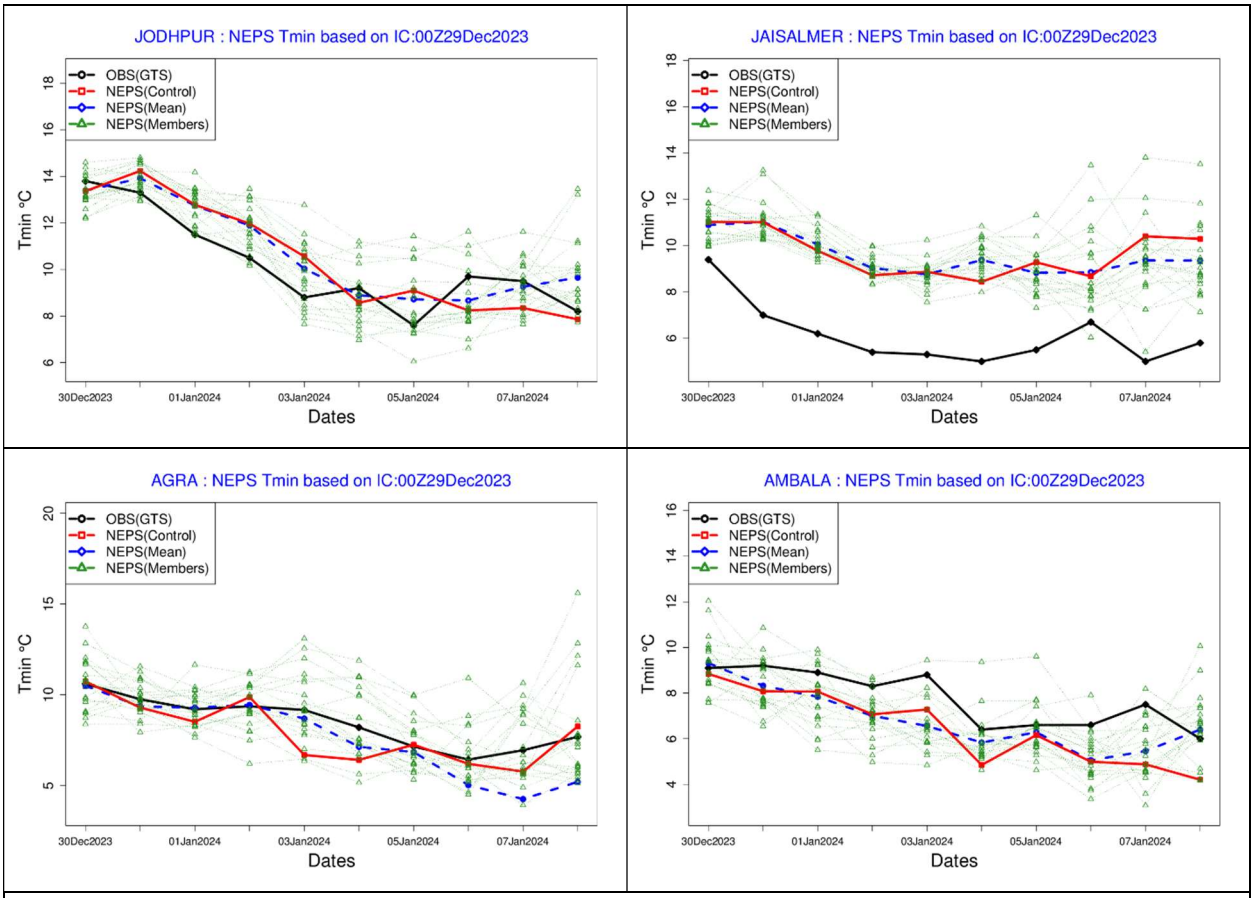

Figure 34. Observed and NEPS-G forecast Tmin over different cities in North India during the cold wave conditions of 29th Dec 2023.

7. Summary and Conclusions

This report documents the performance of the NCMRWF model forecasts during the winter season DJF 2023-24. The verification results are presented to address (a) forecasters and (b) model developers. The information on biases in the forecast winds, temperature, humidity, rainfall, etc., is crucial for the forecasters to interpret the model guidance for forecasting. Additionally, information on recent improvements in the model skill adds to confidence in the model forecasts. The results of the study can be summarized below.

7.1. NCUM-G Mean analysis and anomalies during DJF 2023-24

- *The low-level wind at 850 and 700 hPa shows the presence of anticyclonic circulation over the Central Indian region, indicating high pressure and subdued convection. Penetrating westerlies from higher latitudes having relatively large magnitudes w.r.t ERA5 climatology towards the Indian subcontinent is evident. In the equatorial regions, the upper tropospheric winds are quite weaker.*
- *Low level (850 and 700 hPa) temperature anomalies (against climatology) indicate the winter 2023-24 is warmer with magnitudes between 1-2 ^{0}C in north India. The warmer temperatures stretch from northwest to southeast India, excluding the Indo-Gangetic plains.*
- *DJF 2023-24 indicates a higher percentage of RH compared to the climatology across the entire Indian land region, except for some parts of the northern India region. The Oceanic regions of the Bay of Bengal and Arabian Sea also show positive anomalies in the humidity distribution for the winter period, and negative (positive) anomalies are noted in the equatorial regions at 850 hPa (700 hPa).*

7.2. NCUM-G Systematic Errors

- *Systematic errors in winds at 850 hPa from Day-1 forecasts show an easterly wind bias over the south Bay of Bengal. A westerly wind bias south of the equator around 60^{0}E and an easterly wind bias around the maritime continent (MC) are also noted. With forecast lead time, these errors in low-level winds enhance and this could be due to the enhanced convective activity around the equatorial regions during the winter season. Westerly wind bias is more prominent at 700 hPa level over central India and the northeastern regions in Day-3 and Day-5 forecasts. Systematic errors at 200 hPa level winds show enhanced divergent circulation centred around Kolkata in Day-3 forecasts, and similar spatial patterns in winds are also seen in Day-5 forecasts with enhanced error magnitudes.*
- *Model errors show warm bias (~1 ^{0}C) occupied over most of the Indian land mass, and this bias's magnitude is increasing with forecast lead time. These error increments at 850 hPa temperatures are also more prominent over eastern African regions. On a similar note, temperature errors at 700 hPa also show warm bias (~0.5 ^{0}C) over the northern and central Indian regions. Interesting to see that the bias over the BoB region reverse sign now exhibits cold bias compared to the 850hPa level. Systematic errors at 500 and 200 hPa levels show warm and cold bias, respectively, over the Indian land region, including surrounding oceanic regions.*
- *Systematic errors in RH show a large dry bias over Indian land regions at 850 hPa level, and the dryness is enhancing with forecast lead time. The Omni presence of strong north easterlies over open oceanic*

regions of AS and BoB and increased evaporation could be one primary reason for the positive RH values over these regions. On the contrary, most of the Indian subcontinent and surrounding oceanic regions exhibit moist bias as evidenced by positive RH values, except Africa, the South China Sea, MC, and south of the equator regions. Interestingly the dry bias observed over the Indian land region at 850 hPa level change sign to positive and moist bias is seen at 700 hPa level. Additionally, the moist bias south of the equator is getting intensified in the Day-3 and Day-5 forecast and the entire column is occupied with excess moisture at 700 hPa levels.

- *Systematic errors in surface winds at 10m show North easterlies in Day-1 is changing its direction to southerlies with lead time and it is seen on Day-5. The north-westerly wind bias over northern AS on Day-1 is enhancing its strength with forecast lead time. On a similar note, the easterly wind bias seen in south of the equator around ~100 ^{0}E is also getting intensified with forecast lead time.*
- *Systematic errors in 2m temperature show a relatively warm bias over Indian land regions and north of 40 ^{0}N latitude regions. Interestingly, these warm biases are increasing with forecast lead time, especially over the Indian region. This can be attributed to the dry north-westerly winds from the Northwest entering Indian land and North AS. In addition, most of the oceanic regions of the BoB and AS exhibited warm bias of the range 0-0.5 ^{0}C in all the forecast lead times.*
- *Systematic error in PWAT shows a dryness over the Indian land regions on Day-1, this dryness is enhancing with forecast lead time, and its magnitude is maximum in Day-5. Large positive PWAT biases are seen over BoB, AS, and equatorial regions. This excess column water could be one reason for excess rainfall over these regions.*

7.3. Forecast Verification during DJF 2023-24

- *NCUM-G forecast overestimates rainfall amounts and spatial distribution over oceanic regions around the equator, northeast, and western parts of J & K regions. Rainfall means error (ME) show wet bias over southern parts of the oceanic regions consistent with the mean rainfall patterns. Small dry bias regions are noticed over Sri Lanka, western parts of south BoB, eastern parts of J & K, and some parts of Tamil Nadu in the forecasts, and the magnitude of dry bias increases with lead time.*
- *For different rainfall thresholds (3-30mm/day), POD and FAR show a decrease and increase in scores, respectively. POD >= 0.4 for rainfall up to 3 mm/day. The BIAS score (frequency bias) indicates that forecasts overestimate the frequency of all thresholds. The values of PSS and SEDI all are high for rainfall up to 3-5 mm/day suggesting reasonable skill. PSS score shows a very sharp decrease as the threshold varies. Overall, the skill is not bias-free. For higher rainfall thresholds (> 10 mm/day), frequency bias is almost constant, but the skill is low as indicated by CSI, PSS, and SEDI.*
- *Interestingly the POD and PSS scores for Tmin thresholds remain nearly constant up to 20-22 ^{0}C with values less than 0.4. However, the PSS scores slightly increase at rainfall 22-24 ^{0}C. FAR scores over India as whole shows relatively large values >0.6 up to temperature thresholds 20-22 ^{0}C, later a gradual decrease is noticed in all the forecast times.*

7.4. Verification for Significant Weather Events during DJF 2023-24

Bay of Bengal SCS 'Michaung' (01-06 Dec 2023), Western Disturbances, extreme rainfall events, and Cold waves formed significant weather events of DJF 2023-24.

- ***Initial Position Error**: Mean initial position errors are lower in NCUM-G (32 km).*
- ***Direct Position Error**: NCUM-G and NEPS-G show track errors less than 100 km up to 60 hrs. NCUM-R shows the highest track error for all the lead times.*
- ***Landfall Position & Time error**: The landfall position errors <50 km is seen from from NEPS-G after 2nd Dec. The landfall time error ~ 3 h in NCUM-G for ICs 2nd and 3rd Dec. There was an accurate prediction of landfall time from NEPS-G on 3rd (12 UTC) and 4th (00 UTC) Dec.*
- ***Intensity verification (NCUM-G & NCUM-R)**: MAE in CP is lower in NCUM-R but higher in MSW.*
- ***Verification of strike probability (NEPS-G)**: The ROC curves show that the models have reasonably good skill (ROC is 0.84).*
- ***The spatial verification** of Day-3 & Day-5 rainfall valid on 4th and 6th Dec 2023 corresponding to SCS 'Michaung' consistently indicates eastward and northward shift in forecasts. While the object parameters (area, mean rainfall, highest amount, and volume) for the 40mm/day threshold (over the sea) suggest forecasts underestimate, for 20mm/day CRA (over land), the forecasts underestimate. The forecast error is mainly contributed (>50%) by the pattern error.*
- *For the **Western Disturbance**, the forecast shows an accurate prediction of the trough in the westerlies at 500 hPa up to 5 days ahead. Associated low temperatures are accurately predicted in the NEPS-G ensemble mean. Ensemble members have a reasonable spread around the observations indicating reliability in ensemble forecasts.*

References

1. Ashrit, R., Elizabeth Ebert, Ashis K. Mitra, Kuldeep Sharma, Gopal Iyengar and E.N. Rajagopal 2015a: Verification of Met Office Unified Model (UM) quantitative precipitation forecasts during the Indian Monsoon using the Contiguous Rain Area (CRA) method. NMRF/RR/03/2015.
2. Ashrit R, Sharma K, Dube A, Iyengar G R, Mitra A K and Rajagopal E N 2015b: Verification of short-range forecasts of extreme rainfall during monsoon; Mausam 66 375–386, 607.
3. Barker, D., 2011. Data assimilation-progress and plans, MOSAC-16, 9-11 November 2011, Paper16.6.
4. Ebert, E.E. and W.A. Gallus, 2009: Toward better understanding of the contiguous rain area (CRA) method for spatial forecast verification. Wea. Forecasting, 24, 1401-1415.
5. Hersbach H, Bell B, Berrisford P, et al. 2020: The ERA5 global reanalysis. Q J R Meteorol Soc. 2020;146:1999–2049. https://doi.org/10.1002/qj.3803
6. Jolliffe, I. T., and D. Stephenson, 2012: Forecast Verification: A Practitioner's Guide in Atmospheric Science, John Wiley & Sons, Ltd.
7. Kumar Sumit, A. Jayakumar, M. T. Bushair, Buddhi Prakash J., Gibies George, Abhishek Lodh, S. Indira Rani, Saji Mohandas, John P. George and E. N. Rajagopal 2018: Implementation of New High Resolution NCUM Analysis-Forecast System in Mihir HPCS. NMRF/TR/01/2019, 17p.
8. Kumar Sumit, Gibies George, Buddhi Prakash J., M. T. Bushair, S. Indira Rani and John P. George 2021: NCUM Global DA System: Highlights of the 2021 upgrade, NMRF/TR/05/2021.
9. Kumar Sumit, M. T. Bushair, Buddhi Prakash J., Abhishek Lodh, Priti Sharma, Gibies George, S. Indira Rani, John P. George, A. Jayakumar, Saji Mohandas, Sushant Kumar, Kuldeep Sharma, S. Karunasagar, and E. N. Rajagopal 2020: NCUM Global NWP System: Version 6 (NCUM-G:V6), NMRF/TR/06/2020
10. Mitra, A. K., A. K. Bohra, M. N. Rajeevan and T. N. Krishnamurti, 2009: Daily Indian precipitation analyses formed from a merged of rain-gauge with TRMM TMPA satellite derived rainfall estimates, J. of Met. Soc. of Japan, 87A, 265-279.
11. Mitra, A. K., I. M. Momin, E. N. Rajagopal, S. Basu, M. N. Rajeevan and T. N. Krishnamurti, 2013, Gridded Daily Indian Monsoon Rainfall for 14 Seasons: Merged TRMM and IMD Gauge Analyzed Values, J. of Earth System Science, 122(5), 1173-1182.
12. Sharma K., S. Karunasagar and Raghavendra Ashrit 2020: CRA Verification of GFS and NCUM Rainfall Forecasts for Depression cases during JJAS 2018. /NMRF/RR/05/2020
13. Sharma, K., Ashrit, R., Kumar, S. et al. Unified model rainfall forecasts over India during 2007–2018: Evaluating extreme rains over hilly regions. J Earth Syst Sci 130, 82 (2021). https://doi.org/10.1007/s12040-021-01595-1
14. Srivastava A K, Rajeevan M and Kshirsagar S R 2009: Development of a high resolution daily gridded temperature data set (1969–2005) for the Indian region; Atmos. Sci. Lett. 10 249–254, https://doi.org/10.1002/asl.232
15. Stephenson D.B., B. Casati, C.A.T. Ferro and C.A. Wilson, 2008: The extreme dependency score: a non-vanishing measure for forecasts of rare events. Meteorol. Appl., 15, 41-50.
16. Walters, D., and co-authors: The Met Office Unified Model Global Atmosphere 6.0/6.1 and JULES Global Land 6.0/6.1 configurations, Geosci. Model Dev., 10, 1487–1520, https://doi.org/10.5194/gmd-10-1487-2017, 2017
17. Wilks D S 2011 (eds) Statistical methods in the atmospheric 807 sciences; 3rd edn, Elsevier, 676p

Appendix-I

A1. Brief Description of NCMRWF Models

(i) NCMRWF Unified Model (NCUM-G, NCUM-R, NEPS-G and NEPS-R)

Table-A1: NCMRWF Unified Model Configuration

Model	Application & Domain	Resolution	Forecasts	Track Prediction
NCUM-G	Global NWP Forecasts	N1024L70 (12km horizontal resolution with 70 vertical levels)	00UTC: Day0 to Day10 12UTC: Day0 to Day 10	Up to 120 h
NEPS-G	Global Ensemble Prediction	N1024L70 (12 km horizontal resolution; Control+ 11 member)	00UTC: Day0 to Day10 12UTC: Day0 to Day10	Up to 120 h
NCUM-R	Regional domain (5-40°N and 65-100°E)	4 km resolution Explicit convection	00UTC: Day0 to Day3 12UTC: Day0 to Day3	Up to 72 h
NEPS-R	Regional Domain (7-38°N and 67-98°E)	4 km resolution (Control+ 11 member) Explicit convection	00UTC: Day0 to Day3	Up to 72 h